A Parametric Analysis of the Start-up Procedure and Flight Characteristics of a Gliding Autogyro

by

Michael Oliver

Submitted to the Department of Aeronautics and Astronautics
in partial fulfillment of the requirements for the degree of

Master of Science in Aeronautics and Astronautics

at the

MASSACHUSETTS INSTITUTE OF TECHNOLOGY

February 2005

Author .....
Department of Aeronautics and Astronautics
January 14, 2005

Certified by .....
Wesley L. Harris
Professor of Aeronautics and Astronautics
Thesis Supervisor

Certified by .....
Timothy M. Barrows
Principal Member Technical Staff, Draper Laboratory
Thesis Supervisor

Accepted by .....
Jaime Peraire
Chair, Committee on Graduate Students

DISCLAIMER NOTICE

The accompanying media item for this thesis is available in the MIT Libraries or Institute Archives.

Thank you.

[This page intentionally left blank.]

A Parametric Analysis of the Start-up Procedure and Flight Characteristics of a Gliding Autogyro

by

Michael Oliver

Submitted to the Department of Aeronautics and Astronautics
on January 14, 2005, in partial fulfillment of the
requirements for the degree of
Master of Science in Aeronautics and Astronautics

Abstract

Currently, Draper Laboratory is in the development stages of a gliding autogyro airdrop system. The goal of the project is to design a platform capable of placing small, high value items into urban terrain. Theoretically, autogyros can achieve descent rates and glide slopes similar to current parafoil based systems, but do so with greater precision.

Over the past half-century most rotorcraft research has focused on helicopter design, only viewing autorotation as a means of achieving emergency landings. In contrast, this project utilized early rotor theory to develop algorithms which can predict unpowered rotor performance across the entire flight envelope. To validate these predictions, a vertical wind tunnel capable of testing rotors up to 4 feet in diameter at descent rates of up to 25 ft/s was constructed. Emphasis was also placed on developing deployment sequences that would allow the system to achieve stable autorotation autonomously.

By varying parameters such as blade pitch angle and rotor solidity, it is shown that in the proper configuration, rotor based systems can match and even surpass parafoils in areas such as descent rate and glide slope. The autogyro also has the added capability of varying its lift-to-drag ratio in flight while maintaining reasonable descent speeds, allowing for more precise control to the target. Possible deployment sequences are displayed, proving that relatively simple configurations can be brought into stable autorotation. The algorithms developed and vertical wind tunnel constructed for this project can be used to gain further knowledge of autogyro performance.

Thesis Supervisor: Wesley L. Harris
Title: Professor of Aeronautics and Astronautics

Thesis Supervisor: Timothy M. Barrows
Title: Principal Member Technical Staff, Draper Laboratory

Acknowledgments

I would first like to thank my advisor, Tim Barrows. No matter how often I stopped by his office, he was always willing to take a few minutes out of his day to listen to my ideas. The same can be said of Sean George. Sean probably added as many ideas to this project as is possible without getting to sign the title page. Also at Draper Laboratory, I thank Neil Barbour and Jamie Anderson for trusting me enough to let me try and build a wind tunnel, and Tome Howe for helping me build it.

At MIT I thank Professor Wesley Harris, who was willing to take on another student while running an entire department. I also thank Mark Spearing, my original MIT advisor, who pointed me in the right direction when I first checked in.

Finally, I'd like to thank both the Draper Laboratory and MIT's Aero/Astro program for funding my education, the Navy for letting me come to MIT, my parents for encouraging me to do whatever I enjoy, and my friends for taking my mind off work on the weekends.

Contents

[This page intentionally left blank.]

List of Figures

List of Tables

[This page intentionally left blank.]

List of Symbols

A ..... area

AR ..... aspect ratio

CFM ..... cubic feet per minute

C_Q ..... torque coefficient $\frac{Q}{\pi R^3 \rho(\Omega R)^2}$

C_T ..... thrust coefficient $\frac{T}{\pi R^2 \rho(\Omega R)^2}$

C_0 ..... pressure loss coefficient (Section 3.1.2)

D ..... drag

DOF ..... degrees of freedom

F ..... thrust coefficient based on resultant velocity $\frac{T}{2\pi\rho R^2 U}$

I_B ..... body moment of inertia

I_R ..... rotor moment of inertia

L ..... lift

L/D ..... lift-to-drag ratio

Q ..... rotor-shaft torque

R ..... rotor radius

R_f ..... resultant force

R_p ..... porosity

Re ..... Reynolds number

RPM ..... rotations per minute

T ..... thrust

U ..... resultant velocity through rotor disk

V ..... total velocity

V_v ..... descent velocity

W ..... weight

a_v ..... vertical acceleration

b ..... number of blades

c ..... blade chord

c_{d_B} ..... blade drag coefficient

c_{d_R} ..... rotor drag coefficient $\frac{T}{.5\rho V_i^2 \pi R^2}$

c_{l_B} ..... blade lift coefficient

c_{l_α} ..... lift curve slope

f ..... thrust coefficient based on descent velocity $\frac{T}{2\pi\rho R^2 V_i^2}$

g ..... gravitational constant

m ..... mass

p ..... pressure

r ..... blade section radial distance

x ..... characteristic length

Ω ..... angular velocity

α_B ..... blade angle of attack

α_R ..... rotor angle of attack

δ ..... blade mean drag coefficient

θ ..... blade pitch

λ ..... inflow ratio (Eqn. 2.9)

μ ..... tip speed ratio (Eqn. 2.16)

μ_v ..... viscosity

ν ..... induced velocity

ρ ..... density

σ ..... rotor solidity (Eqn. 4.1)

ϕ ..... inflow angle (Eqn. 2.4)

Chapter 1

Introduction

Recently, Draper Laboratory has been working to develop precision air drop systems. Thus far, the work has mainly focused on developing GPS guided parafoils to enhance the accuracy of traditional parachute based platforms. However, over the past year research has begun on a new concept, an autogyro based airdrop system.

Utilizing the same theory that allows helicopters to make emergency landings and maple trees to spread their seeds for hundreds of feet, this concept replaces the parachute with a helicopter rotor. Under the correct conditions, an unpowered, "autorotating", rotor can produce descent rates similar to a parachute of the same area, but with enhanced controllability. This improvement is an enormous advantage on the modern battlefield where combat is increasingly taking place in urban areas, where even ten feet of error can mean the difference between delivering the payload to the target or hitting a high rise building.

1.1 Background

Of late, military audiences have been inundated with two buzz words: autonomy and precision. Autonomy is defined as "the state or quality of being independent." [9] In military terms, this means that a system has the ability to act without a human operator present, or in layman's terms: computer controlled systems. Precision is simply defined as "characterized by accurate action." [9]

Attempting to create systems that are both autonomous and precise is a difficult task. In well defined scenarios, computers operate much more accurately and efficiently than humans. Areas such as assembly lines and grocery markets have already begun to replace human workers with autonomous systems. However, the battlefield has never been characterized as a well defined scenario. As much as military leaders would like to automate every system, therein reducing the risk to American lives, the dangers in doing so are still too great. An automated system cannot be precise in its actions if it does not know what it is supposed to do, and computers are still far behind humans when it comes to creativity.

Nevertheless, as computing speed continues to increase and computer programmers continue to improve, computers are making their way more and more onto the battlefield. The initial steps have already been taken with unmanned aerial vehicles (UAV) such as the Predator and Global Hawk. Currently, these aircraft are used mostly for reconnaissance purposes, where mistakes are not as costly in terms of equipment and lives.

The next step in their evolution is to use UAVs to autonomously deploy payloads. Initial work has focused on using the Predator UAV to deploy ground based sensors. By using UAVs to set-up ground based sensor networks, commanders can gather vital information about enemy position and movement at no risk to friendly troops. However in order to utilize these sensors, there needs to be an airdrop system capable of placing a payload extremely accurately.

Sensor networks are only one possible use of precision air drop systems. Another is resupplying troops engaged in battle. To improve troop safety, the accuracy of air delivery systems needs to be improved to the point where the soldiers on the ground do not have to break cover to retrieve the supplies. Other missions ranging from weapons delivery to humanitarian aid, show that anything that dropped from the sky can benefit from being dropped more accurately.

1.2 Precision Air Drop

Almost as soon as man learned to fly, he began dropping things from the sky. There are few people alive who have not seen images from the Second World War of thousands of soldiers pouring out of C-47s or modern pictures of aircraft dropping food and supplies into hostile regions. The parachutes used in both cases did no more than simply slow the descent rate of the payload to a safe speed, and the paratrooper or package was left to float with the wind. Eventually some control was added for paratroopers, but only so much as to turn to the desired direction and overcome a slight wind.

More recently, the parachute has been replaced by the parafoil, which gives expert users good control over flight direction. This allows well trained soldiers to choose their landing spot by adjusting their descent path in accordance with the wind. On a day with moderate winds, the best jumpers in the world can hit a ten yard wide circle. However, autonomously guided parafoils have not yet achieved this type of accuracy.

Recent military operations have focused on asymmetric warfare. There is no longer a world power which can match the United States in open battle for an extended period of time. Thus in order to negate our warplanes and tanks, enemy troops have chosen to fight guerrilla warfare, hiding themselves in caves and civilian occupied buildings. In order to utilize our technological advantage in these arenas, the accuracy of airdrop platforms needs to improve.

Currently the only UAV deployable parafoil system is Stara Technolies' GNAT. [5]. This system is capable of deploying a payload between one and four hundred pounds from a UAV. It then uses GPS to guide it down to the target. Although its exact accuracy and range are not published, it is known that the GNAT approaches the target in a 100 foot radius spiral. Thus at worst, its accuracy is approximately 30 meters. It can be assumed the impact accuracy is slightly better than this.

As of now, the GNAT has a monopoly on the small-payload, precision airdrop market. This nearly empty market leaves plenty of room for additional competitors

to field new products. By approaching airdrop from an entirely new perspective, the autogyro based system may be able to earn a place alongside the GNAT as a viable option for military commanders.

1.3 History of the Autogyro

Although a novel idea in the field of airdrop, the concept of the autogyro is far from new. The oldest example of autorotation can be seen as a maple seed spins to the ground. As it falls, the aerodynamic forces acting on the seed cause it to spin. The spinning in turn creates a lifting force, which not only slows down the descent rate of the seed, but also allows it to glide away from its parent tree.[16]

Science caught up with nature in the early 20th century when various physicists began to study the aerodynamics of rotation more closely. Boris Yur'ev of Russia coined the term "auto gliding". Yur'ev's lab performed tests on model helicopter rotors to display how an unpowered rotor could be made to turn on its own under certain descent conditions. While helicopter designers were still determining how to overcome the torque produced by a powered helicopter, engineers focused on autorotation were consistently improving the basic rotor theory.[16]

In the 1910's, the autogyro found its champion in Juan de la Cierva. While other engineers viewed autorotation only as an aid in designing the powered helicopter, de la Cierva felt that an aircraft could be designed in which the rotor was never powered. His initial design was a model sized glider. De la Cierva can be seen holding his glider in Fig. 1-1.

The glider seen in Fig. 1-1 shows striking similarities to the test article, which was used in this project over eighty years later. Eventually de la Cierva focused his attention on a powered autogyro, which he patented as the *Autogiro*. By using a free spinning rotor in place of a wing, and adding a conventional aircraft propeller to provide thrust, the Autogiro was capable of achieving level flight.[8] The first operational rotorcraft, the Autogiro proceeded the helicopter by over a decade.

De la Cierva was most impressed by what he deemed the stall-proof nature of

Figure 1-1: Juan de la Cierva with his gliding autogyro.[16]

the autogyro. While a conventional aircraft must maintain forward flight to provide lift, the autogyro could safely make a near vertical descent. Unfortunately for de la Cierva, the invention of the anti-torque tail rotor made powered helicopters feasible, and the autogyro was downgraded to a second rate aircraft.

Eighty years later, the autogyro has a chance to re-emerge. Combining the simple glider designed by de la Cierva with a modern control system, someday rotor based airdrop systems could be as common as the parachutes used today. When comparing the relative merits of the two, the autogyro has its advantages and disadvantages, which later will be discussed in depth. If its pros eventually outweigh its cons, airdrop may just be the break the autogyro needs to regain its reputation among flying vehicles.

1.4 Objectives

Draper Laboratory's overall goal is to develop an autogyro based airdrop system. With that in mind, this project takes the first steps towards that goal by determining first, what technology it will take to autonomously deploy the system. Then, the

overall performance of the system will be evaluated through a parametric analysis to determine if it truly can compete with parafoil based systems.

This research intends to answer the following questions:

- What type of flight performance can be achieved by a gliding autogyro?
- Can a fixed pitch rotor can be deployed with its blade pitch set in the rotor "working state"?
- What is the added benefit of including collective control in the rotor hub design?

1.5 Thesis Outline

Chapter 2, *Background and Theory*, describes the theoretical aspects of the project. Topics covered range from the basic theory of autorotation to the complications of rotor start-up and flight performance algorithms. This chapter provides the necessary background to fully understand the material discussed in Chapters 4 and 5.

Chapter 3, *Experimental Setup*, is a description of how the Draper Vertical Wind Tunnel was designed and constructed. Aspects of wind tunnel design and construction such as flow losses and tunnel calibration are discussed. This chapter also covers the design of the test autogyro, which was used to validate the hypotheses of the project.

Chapter 4, *Theoretical Performance Evaluation*, uses the algorithms laid out in Chapter 2 to perform a parametric analysis on the flight performance of a gliding autogyro. By automating the basic algorithms of A.A. Nikolsky, S.E. Slaymaker, and F.J. Bailey, the effects of blade pitch and rotor solidity on flight performance are evaluated based on such indices as descent speed and lift-to-drag ratio.

Chapter 5, *Experimental Results*, begins by determining the accuracy and precision of the Draper Vertical Wind Tunnel. Once the system is deemed to be accurate, the chapter shifts its focus to a comparison between theoretical results and experimental data. Also discussed are the complications of starting the rotor during descent based on blade pitch control.

Chapter 6, *Conclusions*, briefly discusses the project as a whole. Focus is placed on the benefits of having collective, as well as the overall usefulness of such a system. It concludes by discussing areas which must be further explored before a gliding autogyro system could be drop tested.

[This page intentionally left blank.]

Chapter 2

Background and Theory

In order to fully understand how the autogyro works, it is necessary to have a general understanding of rotor aerodynamics. Simply understanding how lift and drag act on an airfoil is half the battle when it comes to basic rotor aerodynamic theory. Rotor performance can be predicted for almost all flight states using a series of equilibrium conditions. Unfortunately, these equilibrium conditions are dependent upon the other significant factor affecting autogyro performance: induced velocity. Unlike lift and drag, the induced velocity is not a simple concept. However, it must be understood if one is attempting to create any type of rotorcraft.

As this project also focuses on the complications of achieving autorotation, the start-up procedure is examined from a theoretical standpoint. This section deals with more complex aerodynamic properties such as the Reynolds number and post-stall characteristics of the rotor blades.

2.1 Basic Autorotation Theory

As mentioned earlier, in its simplest form autorotation is based on equilibrium. A given blade section has an equilibrium angle of attack. This point leads to an equilibrium RPM for the entire blade. This RPM produces a given thrust, which finally gives the equilibrium descent velocity of the entire autogyro system. In vertical flight, the aerodynamic forces acting on each element in the system remain constant for a

given trim condition. In forward flight, these forces vary as each blade rotates around the shaft. However, in both cases the trim conditions can be viewed as a static problem if the correct assumptions are made. Before system trim conditions and rotor performance can be analyzed, it is necessary to first look into the forces acting on the individual blades.

2.1.1 Blade Section Equilibrium

Although lift and drag may be considered as some of the most simple aerodynamic concepts, many times they are not fully understood. Often lift is viewed as the force acting up, and drag is the force pulling back. In the case of an airplane wing, this is true for steady, level flight. However, autorotation relies on the exact definition of lift and drag.

> Lift: the aerodynamic force acting normal to the relative wind
>
> Drag: the aerodynamic force acting parallel to the relative wind[2]

The key phrases here are, "normal/parallel to the relative wind." Unlike the wing of an airplane, rotorcraft not only gain a component of relative wind from their flight speed, but also from the rotation of the rotor. Thus, the wing of an aircraft falling straight down at 20 ft/s, only sees a relative wind of 20 ft/s. However, the blade of an autogyro sees a vertical component of 20 ft/s and a varying horizontal component that depends on RPM and radial location on the blade. This introduces two fundamental properties of autorotation: the induced velocity, ν and inflow angle, ϕ.

To produce thrust, rotorcraft must either force air downwards (helicopters), or slow down the air flowing through the rotor disk (autogyros). The change in speed of the airflow, either positive or negative, is known as the induced velocity. Thrust produced by a rotorcraft is highly dependent on induced velocity. For instance, in the normal working state of a rotor the total thrust is calculated as:

$$T = \pi R^2 \rho(\nu + V_v)2\nu \tag{2.1}$$

Where V_v is the climb velocity of the rotorcraft. Eqn. (2.1) shows that thrust is proportional to $(\nu + V_v)\nu$.[11] This demonstrates how important it is to obtain an accurate value for the induced velocity.

The inflow angle is defined as:

$$\phi = \alpha_B - \theta \tag{2.2}$$

where θ is the blade pitch angle, and α_B is the blade angle of attack. Because the blade pitch is usually fixed for a given state, the blade angle of attack is dependent mostly on the inflow angle, which in turn is dependent on the descent speed, induced velocity, and angular velocity of the blade section. Thus, if angular velocity and descent speed are known, the inflow angle can be obtained from the induced velocity, or vice versa. This is an important fact when calculating equilibrium conditions because once the inflow angle is known, the angle of attack is known, and rotor performance can be determined.

This is not an easy process to complete, as induced velocity is also a function of RPM, and angular velocity varies along the blade itself. This type of problem is known as an implicit equation. In past analysis, this complication has led to iterative schemes to calculate rotor performance. The most elementary analysis of equilibrium occurs at the blade section level. Fig. 2-1 shows the forces acting on a blade section in autorotation.

In Fig. 2-1, the arrows labeled U show the vertical component of the relative wind, which is caused by the descent speed minus the induced velocity. The arrow labeled Ωr is the component of relative wind caused by the rotation of the blade. Summing these two components gives the actual relative wind as seen by the blade section. In the following analysis, it is assumed that the rotor shaft is vertical.

As mentioned before, one must be careful in how lift is defined. This is because lift on an autogyro blade does not act straight up. Rather it acts normal to the relative wind, at an angle of ϕ forward of the vertical plane of the rotor. Likewise drag acts at an angle of ϕ off the horizontal plane of the rotor disk. This fact allows for

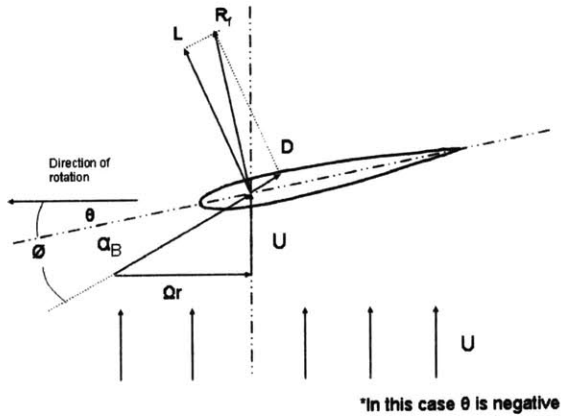

Figure 2-1: Aerodynamic forces acting on a blade section in autorotation.

autorotative equilibrium to occur. A blade section is considered to be in equilibrium when the horizontal components of drag and lift are equal.

$$Horizontal\ force\ = Lsin(\phi) - Dcos(\phi) \tag{2.3}$$

If the horizontal component of lift is greater, the blade section is considered an accelerating section because the forces want to pull the blade forward and increase RPM. If the horizontal component of drag is greater the opposite occurs.

The inflow angle thus has a stabilizing effect on Eqn. (2.3). As the blade accelerates the inflow angle decreases, causing the lift term in Eqn. (2.3) to decrease and the drag term to increase. If the blade decelerates, the opposite will occur. In vertical descent, inflow angle is defined as:

$$\phi = tan^{-1}\frac{V_v - \nu}{\Omega r} \tag{2.4}$$

For a given blade section, the equilibrium inflow angle can be calculated by:

$$\phi_{eq} = tan^{-1}(\frac{c_d}{c_l}) \tag{2.5}$$

If the inflow angle is then plotted on the vertical axis and angle of attack is plotted on the horizontal axis Fig. 2-2 can be obtained.

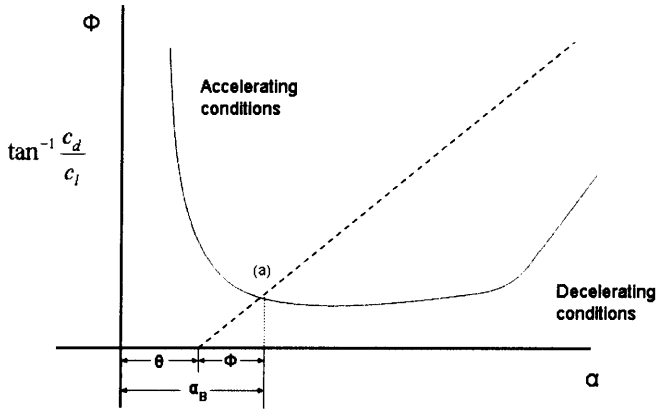

Figure 2-2: Equilibrium conditions for a blade section, positive θ.

Because the vertical axis is inflow angle, and angle of attack is calculated as blade pitch plus inflow angle, a 45^o line can be drawn from the blade pitch value on the horizontal axis, which will define the blade operating conditions. As Fig. 2-2 shows, for a given pitch there are three possible operating conditions for the blade section: accelerating, decelerating, or equilibrium. Which condition the blade section is in depends on the inflow angle. For low inflow angles, $Lsin(\phi)$ is small and the conditions are decelerating. On the other hand, high inflow angles cause accelerating conditions. Point (a) where Eqn. (2.5) holds true defines the equilibrium inflow angle.

To obtain the best lift-to-drag ratio for a blade section, the minimum of Eqn. (2.5) would be taken, and drawing a a 45^o line from the equilibrium point back to the horizontal axis would determine the pitch. To obtain the blade pitch for the minimum power condition, the angle of attack for minimum power, $c_{d_0}/c_l^{3/2}$, would be calculated. Then, the equilibrium inflow angle for this angle of attack would be determined from Eqn. (2.5). Finally, a 45^o line drawn from the equilibrium point to the horizontal axis would determine the blade pitch.

2.1.2 Blade Equilibrium

Note that everything discussed to this point has only been concerned with the characteristics of a single blade section. During autorotation, each blade section sees a different velocity, due to differing radial positions and induced velocities. These changing quantities will cause the inflow angle, and thus angle of attack, to vary along the span of the blade. Fig. 2-3 shows the effect of inflow angle variation across the span of the blade.

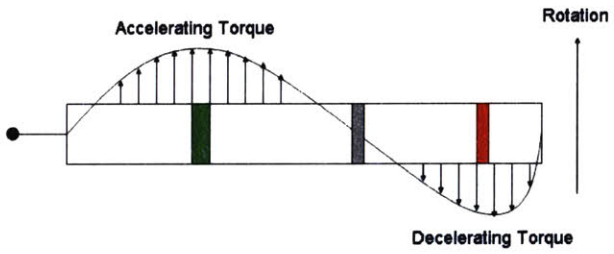

Figure 2-3: Equilibrium conditions across blade span.

On the inner portion of the blade, where the angular velocity is small, and the inflow angle is high, accelerating conditions exist. On the outer portion of the blade, the angular velocity is high, which results in a small inflow angle and decelerating conditions. The only section truly in equilibrium occurs at approximately 75% of the span. The entire blade is in equilibrium when the sum of the accelerating and decelerating torques is equal to zero.

Fig. 2-3 holds true for all rotor blades. However, if twist is used to vary the pitch along the blade span, the angle of attack at the various radial positions can be controlled to optimize the rotor performance.

By understanding the basic principles of autorotation, it is possible to determine

what rotor parameters affect performance. Obviously, lift and drag characteristics come to mind. These parameters are mostly affected by the airfoil section chosen and blade geometry. Inflow angle is another important parameter, and the easiest way to control the inflow angle is with blade pitch. Thus, the first step in designing an autogyro system is to determine which airfoil cross-sections, blade geometry, and blade pitches provide the best performance.

2.2 Complications of Start-up

Most autorotation theory is concerned with rotors already in equilibrium. This means the blade is spinning freely and providing thrust to the system. Due to the nature of the proposed system, the autogyro rotors will not initially be rotating. Instead they will begin in a locked position where $\alpha_B = 90^o$, and the entire system is stalled. Obviously this is outside of normal rotor dynamics.

During this time, the rotor will be in a controlled descent due to the attached parachute. However, it will not be operating in the flow regime for which most rotors are designed. Instead, theory for the start-up procedure must be developed. Operation in this "post-stall" area is hard to predict accurately, but it is possible to gain a general understanding of the factors affecting start-up.

2.2.1 Effect of Blade Pitch on Start-up

On page 27, Fig. 2-2 was used to describe the forces acting on a blade section at various inflow angles. For the purposes of stable autorotation, this diagram works, but in order to describe the full range of autorotation possibilities, it must be extended to cover all values of inflow angle. Fig. 2-4 does this.

The green box in the lower left-hand corner of Fig. 2-4 is actually Fig. 2-2. From this box, the horizontal axis has been extended to show blade angles of attack from 0^o to 180^o. Likewise the vertical axis has been extended to show inflow angles ranging from 0^o to 180^o. This covers the full range of possible autorotative rotor states.

The blue curve represents the equilibrium inflow angles, which are solutions to

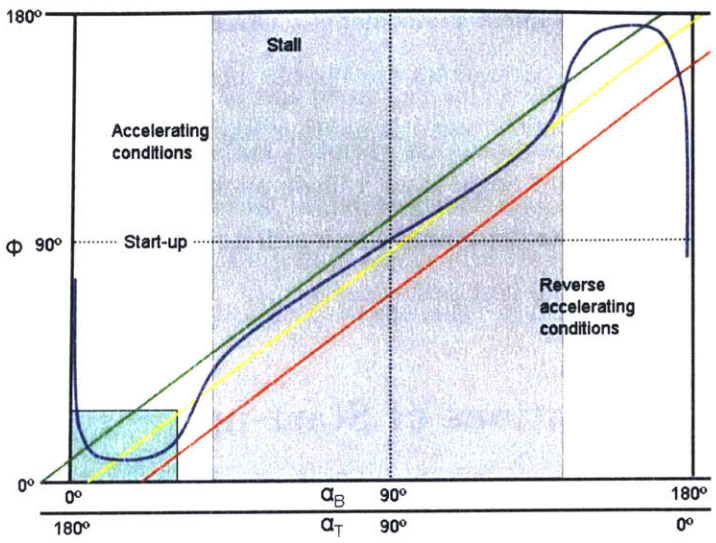

Figure 2-4: Full range of equilibrium conditions for a blade section.

Eqn. (2.5). However, it is extended to show all possible angles of attack from 0 to 180^o. Extending the theory this far has its difficulties. For instance, the grey box represents the stalled region of flow. In these post-stall regions, values for c_d and c_l are not consistent, and the shape of the blue curve is not well defined. Also operating at $\alpha_B = 180^o$ is the same as operating at $\alpha_T = 0$, where α_T is reference to the trailing edge of the blade. This fact can be seen by the dual angle of attack scales along the x-axis of Fig. 2-4. To better understand α_B and α_T, Fig. 2-5 shows the relationship between the two for a given velocity.

The portion of Fig. 2-4 to the right of the grey box is actually similar to the left-hand side, except that it represents the characteristics of the airfoil flying trailing edge forward. For instance, $\alpha_B = 175^o$ is actually representative of the trailing edge flying at $\alpha_T = 5^o$. This portion of the plot is necessary due to the possibility of the rotor spinning backwards, when the trailing edge in essence becomes the leading edge. For a blade which is symmetrical fore and aft, the blue curve would also be symmetrical.

For a given rotor, any point above the blue curve will represent accelerating conditions; that is conditions which will cause the blade section to be pulled in the desired

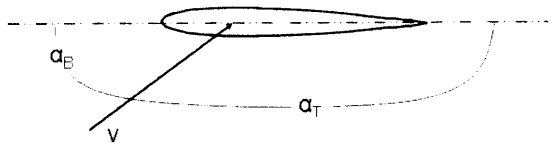

Figure 2-5: Relationship between α_B and α_T.

direction of rotation, increasing the rate of rotation. Below the blue curve are reverse accelerating conditions. These conditions will either slow down a blade spinning in the desired direction, or accelerate a rotor spinning in the wrong direction.

At $\alpha = 0$, the rotor is spinning forward so that the induced velocity is equal to the descent velocity. At $\alpha = 180$, the rotor is spinning backward causing the same effect. At $\phi = 90$, the rotor is not spinning at all. This is the start-up condition.

The red, yellow, and green lines represent possible states for a given blade pitch. Accelerating conditions cause the rotor RPM to speed up in the desired direction, moving the rotor state downward and to the left along the aforementioned lines. Reverse accelerating conditions move the rotor state to the upwards and to right on the lines. Using these curves the nature of the start-up can be determined for a given rotor. Even though these curves are created for blade sections, they can be used to gain a qualitative feel for start-up requirements of the entire rotor.

For example, the green curve represents a rotor with a negative blade pitch. At the start-up point, $\phi = 90^o$, the blade is already in the accelerating conditions and will start to spin forward on its own. Equilibrium is achieved when the green curve intersects the blue curve in the lower left hand corner. This intersection shows what

the equilibrium angle of attack and inflow angle will be for the given pitch.

On the other hand, at start-up the yellow line is in the reverse accelerating conditions. Given the chance to spin backwards this rotor configuration will achieve equilibrium spinning trailing edge forwards. However, if an initial forward RPM is given to the yellow curve so that its inflow angle becomes small enough to cross the blue line into the upper left-hand side of the plot, it will achieve accelerating conditions and reach equilibrium spinning forwards. Once this occurs, the increased pitch becomes a benefit as it results in an increased angle of attack and improved rotor performance.

Finally, the red curve shows a rotor whose blades have too much pitch. At the start-up condition this blade is in the reverse accelerating conditions and will begin to spin backwards. Since the red line never crosses the equilibrium line on the left hand side of the plot, no amount of initial RPM can cause it to reach equilibrium spinning forwards.

These three possible outcomes show the effect of pitch on start-up. Low and negative pitches make start-up easy, however, there is a significant performance sacrifice. High pitches do not even allow the rotor to rotate in the correct direction. Between the two lies a region where start-up is difficult but possible, and here the desired flight performance is achieved.

2.2.2 Effect of Reynolds Number on Start-up

Aside from blade pitch, Reynolds number, Re, effects appear to be the second most significant difficulty to overcome during start-up. Reynolds number is used as a scaling property for aerodynamic behavior and is calculated by:

$$Re = \frac{x\rho V}{\mu_v} \tag{2.6}$$

Where x is a characteristic length for the object, and μ_v is the fluid viscosity.

The effect of Reynolds number on the start-up procedure is due to the fact that low Reynolds numbers, up to approximately 300,000, cause a significant increase in

drag coefficients compared to large Re. For example, Fig. 2-6 shows the effect of Reynolds number on the drag coefficient for a Clark-Y airfoil.

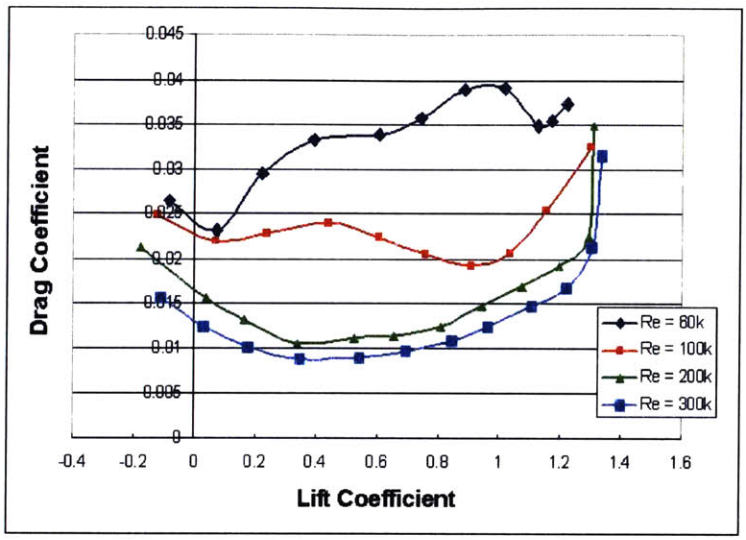

Figure 2-6: Reynolds number effect on c_d[21]

The drag coefficient not only increases as Reynolds number decreases, but its behavior also becomes less predictable. The $Re = 300,000$ curve has the classic parabolic drag polar, but at the lower values of Reynolds number, there is no clear trend to the behavior of the drag coefficient. This erratic behavior of the drag coefficient is not a major problem during start-up, but factors heavily into performance predictions.

As far as start-up is concerned, the increase in the drag coefficient is a significant problem. As shown before in Figs. 2-2 and 2-4, the accelerating and reverse accelerating regions of inflow are based on the ratio between the drag and lift coefficients. If c_d is increased without a corresponding increase in c_l, the size of the accelerating conditions region will decrease as can be seen in Fig. 2-7.

Fig. 2-7 is the left-hand side of Fig. 2-4. The green curve represents a situation where the rotor can achieve autorotation. Given a small enough inflow angle the blue curve, in this case set to 0^o pitch, crosses the green curve and an equilibrium situation will occur.

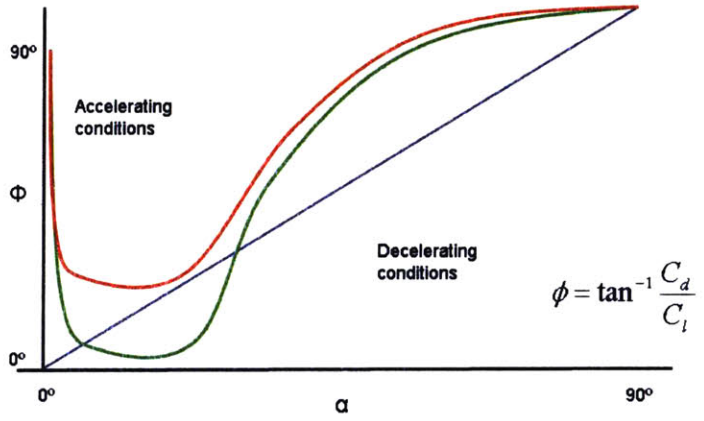

Figure 2-7: Reynolds number effect autorotation curve

On the other hand, the red curve represents the conditions when c_d is increased as with a low Reynolds number. No matter how small the inflow angle becomes, due to Reynolds number effects the blue curve never crosses the red curve and equilibrium cannot be achieved.

2.2.3 Start-up Considerations

Thus far it has been shown that the rotor start-up procedure is affected by blade pitch, airfoil section, inflow angle, and Reynolds number. It can be assumed that the airfoil section will be chosen based on performance and cannot be changed. That leaves blade pitch, inflow angle, and Reynolds number as variables.

The easiest way to start a rotor into autorotation is by pitching the blades down until the inflow curve lies entirely in the region of accelerating conditions. As long as the rotor is equipped with a collective, this would not affect other performance areas. Collective is a system in the rotor, which allows for control of the blade pitch during flight. If instead the blade pitch is to be fixed, as planned in this project, the low pitch value would cause an unacceptable degradation in performance. In this situation the airfoil would have to be started with the pitch value set in the normal

working state of the rotor's performance curve.

The working state of the rotor is defined as the range of blade pitch values that produce near optimum performance. For a common rotor, this covers blade pitches from approximately two to ten degrees. In the working state, as blade pitch is increased two things happen. One, the angle of attack increase, and two, the rotor RPM decreases. These two phenomenon have the effect of canceling each other out in terms of performance. Thus, in the working state overall rotor performance tends to remain fairly constant.

Setting the pitch leaves only inflow angle and Reynolds number effects left as variables. Although in Eqn. (2.4) induced velocity is included in the calculation of the inflow angle, during start-up it can be ignored. This leaves only the descent velocity and the angular velocity as variables. Therefore to obtain a small inflow angle, descent velocity must be decreased and/or RPM increased.

For Reynolds number, the air density and viscosity are uncontrollable. Therefore changes can only be made to the characteristic length and velocity. The characteristic length for an airfoil is the chord, so by increasing chord length, Re can be increased. The total velocity seen by the airfoil is now a factor of the descent velocity and the angular velocity. This means that an increase to either the descent rate or the RPM will increase the Reynolds number.

The initial RPM an autogyro system is capable of attaining is based on the potential energy available to spin-up the rotor. In the current design, this energy is supplied by a spring system, which is wound up prior to deployment and released in mid-flight. The weight restrictions and efficiency of the eventual spin-up system used will dictate how much energy can be transferred to the rotor. Consequently, the maximum initial rotor RPM will be fixed.

After every other variable has been eliminated, the success of the spin-up phase is based on the initial descent speed. Inflow angle considerations would advocate a slow descent speed to produce a low inflow angle. Reynolds number effects would point to a high descent speed to increase the Reynolds number. Obviously as with most aeronautical design problems, the answer lies somewhere in the middle.

2.3 Vertical Flight Performance

One reason the autogyro is superior to the guided parafoil is that the autogyro is capable of achieving vertical flight. Basic predictions place the rotor drag coefficient, c_{d_r}, around 1.2 in vertical flight. The exact value of c_{d_r} can be calculated through a variety of techniques.

The most simple of these are analytical equations. These methods are fast and reasonably accurate. However, they are based on certain assumptions, which may or may not be true. Also due to the complicated nature of the airflow during autorotation, it was necessary to derive a portion of the theory through experimentation. Thus, it can be said that the analytical solutions are actually quasi-experimental.

2.3.1 Analytical Methods

The first steps in analytically determining rotor performance are derived from momentum theory. The process begins with summing the various sources of torque on the rotor and setting this value to zero. From Ch. 6 in *Aerodynamics of the Helicopter* [11], the generalized helicopter power equation is:

$$Power = TV_v + T\nu + \frac{\delta\rho}{8}\Omega R^3 \sigma\pi R^2 \tag{2.7}$$

The first term represents the climb power, or in the case of autorotation, the power gained from descent. The second term is the induced power generated, and the third term is the profile power loss due to the drag of the blades. In the third term, δ is the average drag coefficient of the blades and σ is the solidity ratio of the rotor. These equations can be normalized to give:

$$C_Q = \frac{\delta\sigma}{8} + (\bar{V}_v + \bar{\nu})\frac{C_T^{1.5}}{2} \tag{2.8}$$

The thrust coefficient, C_T, and $\bar{V}_v$ and $\bar{\nu}$, which are the descent and induced velocities normalized by the system's weight, are functions of the inflow ratio. C_Q is the torque coefficient and for the case of autorotation is set equal to zero. From this,

the inflow ratio, which is defined as:

$$\lambda = \frac{V_v + \nu}{\Omega R} \tag{2.9}$$

where α_R is the rotor angle of attack and can be obtained based on the rotor parameters.

Further improvements to Eqn. (2.8) have also been made, to provide more accurate results. One of these improvements was made by John B. Wheatley in NACA Report No. 487. His work added the ability to include tip losses and blade twist into the calculations. He also replaced the averaged drag coefficient term with a parabolic drag polar.[23] These improvements were extremely tedious to calculate until 1938, when F.J. Bailey placed Wheatley's work in a set of tables. This report, NACA Report No. 716, allowed Wheatley's improvements to be used in practical rotor design.[3]

By re-arranging the thrust coefficient in terms of λ and inserting the known rotor parameters into the improved power equation, the equation to be solved is a quadratic in λ with two solutions. For an untwisted blade, Bailey's tables give:

$$0.4704\lambda^2 + 0.3042\lambda\theta = \delta_0\frac{1}{4} + \delta_1\left(\frac{1}{3}\lambda + \frac{1}{4}\theta\right) + \delta_2\left(\frac{1}{2}\lambda^2 + \frac{1}{3}\lambda\theta + \frac{1}{4}\theta^2\right) \tag{2.10}$$

where θ and the parabolic drag coefficients, δ_0, δ_1, and δ_2, are known. In this case, the correct value of λ is the larger value, while the smaller solution corresponds to the rotor operating at a negative angle of attack.[11]

Once λ is known, the rotor RPM can immediately be found based on the blade pitch, lift curve slope, and disk loading. An algorithm for finding RPM, and eventually descent speed, from the inflow ratio was laid out by A.A. Nikolsky and Edward Seckel in NACA Technical Note 1906.[18]

After RPM is determined, the calculations can no longer be made through purely analytical means. To understand why, one must first understand the nature of airflow through a spinning rotor.

The flow states of a rotor can be broken down into three distinct categories: the normal working state, the vortex ring state, and the windmill brake state. The normal working state occurs when "air approaches the rotor in the same direction as the induced velocity."[11] This flow state requires the rotor add energy to the air and is only possible in powered helicopters. The windmill brake state occurs at high rates of descent when the air approaches the rotor in the opposite direction as the induced velocity. During airdrop, when descent rates are required to be small, it is not desirable to enter the windmill brake state.

In autorotation, the ideal situation is to operate in the vortex ring state. Here the freestream and induced velocities are opposite in direction and similar in magnitude. This allows very little flow to pass through the rotor, which results in slow descent speeds. The total upward velocity through the rotor, often called resultant velocity, U, can be defined as:

$$U = -(V_v + \nu) \tag{2.11}$$

where V_v is negative when the rotor is descending. This sign convention is taken from helicopter design where V_v is positive during a climb. During autorotation, $V_v < 0$, $\nu > 0$, and $U > 0$.

When both ν and V_v are positive, the normal working state, or $V_v >> \nu$, the windmill brake state, air travels quickly through the rotor, the flow regime is relatively smooth, and thrust can be calculated based on momentum theory. Unfortunately, the vortex ring state does not have this luxury. When U is small, the rotation of the rotor through the low energy flow causes a significant amount of turbulence. This turbulence causes losses for which momentum theory cannot account.

Instead, experimental data has been taken to relate the resultant velocity to performance for various rotor configurations. This data was then normalized and can now be used to predict the performance for any rotor. Originally developed by Herman Glauert in 1926, the curve was modified by a team from Georgia Tech in 1949.[7] Fig. 2-8 shows both curves.

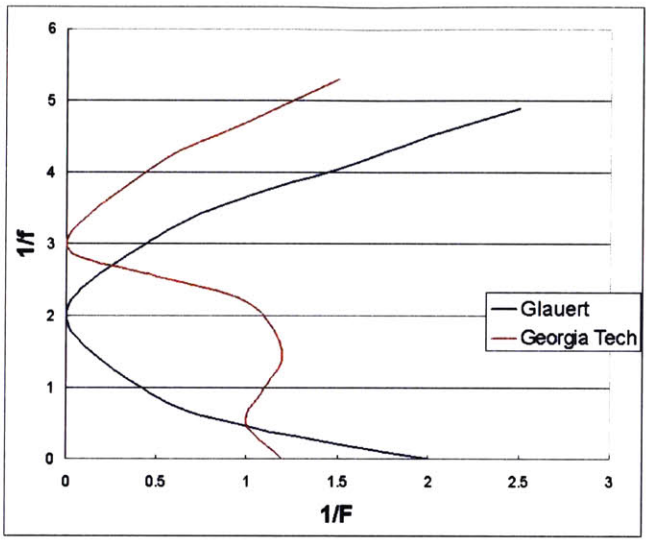

Figure 2-8: Relation between f and F.

The terms F and f are the thrust coefficient based on resultant velocity and descending velocity, respectively. They are defined as:

$$F = \frac{T}{2\pi\rho R^2 U} \tag{2.12}$$

$$f = \frac{T}{2\pi\rho R^2 V_v^2} \tag{2.13}$$

Calculating U from λ and RPM, F can be found. Using F and Fig. 2-8, a value for f can be determined from the curve, and the descent velocity can be found from Eqn. (2.13). Obviously, as Fig. 2-8 shows, there is some disagreement over the relationship between F and f, and the choice of which curve to use significantly effects the performance prediction. This will be analyzed in Ch. 4.

Up to this point, several assumptions have been made, which affect the accuracy of the theory. These are:

- 1 The inflow over the disk is constant.
- 2 The blade drag coefficient can be described by either a constant term or a parabolic curve.

- 3 The blade lift curve is linear.
- 4 The relationship between f and F as seen in Fig. 2-8 is accurate.

More advanced theory, known as the blade element method, has been developed to eliminate the constant inflow assumption. By breaking each blade down into radial sections, the same equilibrium conditions can be solved for at each section producing an inflow that varies radially. If the blade is broken down into an extremely large number of sections, this theory, known as blade element theory, approaches the actual rotor performance. In simple design cases, the extra accuracy gained by using this method does not make up for the extra calculations needed to solve the for equilibrium.

The second and third assumptions play an important role in determining the accuracy of the predictions. The drag term for example has a large influence on equilibrium RPM, which relates directly to thrust. If this term is not described accurately, it will propagate forward through the algorithm to cause eventual inaccuracies in descent rate.

The assumption that the lift curve is linear causes inaccuracies as the airfoils begin to stall. At stall the lift curve should drop off, providing less lift to the airfoil. In terms of autorotation, this translates to less accelerating torque, which will cause the rotor to slow down even further. As shown earlier, there is a fine line between an autorotating rotor and a stalled rotor, and not incorporating an accurate lift curve will tend to blur that line. The danger exists that at higher blade pitches, theory may predict that the rotor should operate correctly, when it will actually be stalled.

2.3.2 Another Semi-Analytical Method

Another semi-empirical method for calculating the steady state descent speed was developed at Princeton University in 1953 by S. Slaymaker and Robin Gray. This theory is not only based on the inflow ratio and resultant velocities, but also calculates the average blade lift coefficient. By determining the lift coefficient on each blade, Eqn. (2.14) can be used as another method of calculating rotor RPM.

$$\Omega = \sqrt{\frac{6W}{\sigma C_l \rho \pi R^4}} \tag{2.14}$$

where W is the weight of the system. Eqn. (2.14) is derived from the equation for vertical acceleration:

$$a_v = g - T/m \tag{2.15}$$

Determining the the effects of the lift coefficient itself had been difficult earlier because it was not the focus of the analysis, but rather a byproduct of the blade pitch and rotor RPM. In contrast, the Slaymaker method focuses initially on the lift coefficient. The drawback to this is that the lift coefficient used is an average lift coefficient for the rotor. Due to the changes in flow properties over the rotor, the true lift coefficient varies radially.

The benefit of the Slaymaker method is that the average lift coefficient shows up directly in the equilibrium equation and can be adjusted. By varying the lift coefficient, which is proportional to blade pitch, in a time step algorithm, the transient behavior of the autogyro's vertical descent performance can be ascertained. This method can be used to determine how beneficial rotor collective will be.

For instance, adding a step or ramp input in the lift coefficient would simulate the effects of flaring the collective in vertical descent, and a decrease in both descent rate and rotor RPM would be seen in the transient behavior. This method could then be used to determine if a collective flare is a viable maneuver during the landing phase of the flight.

Within this algorithm there are a number of constants, which were experimentally determined. Similar to the Nikolsky and Bailey algorithms, Fig. 2-8 is used to determine the inflow ratio. Also, data from tests performed at Princeton in 1953 are used to improve the decelerating torque and transient lift coefficient equations contained within the algorithm. The correctness of of these improvements will significantly affect the accuracy of the performance predictions, and unfortunately, it is extremely difficult to validate the accuracy of their tests.

In conclusion, the Slaymaker method has its uses, as well as its flaws. However, unlike the methods previously mentioned, it allows for analysis of the transient behavior. Thus, if used correctly, the Slaymaker method can provide an analysis capability the more classical theories lack.

2.3.3 A Comparison of the Semi-analytical Algorithms

Thus far, three different algorithms have been listed: the Nikolsky, Bailey, and Slaymaker. All three algorithms are based on theory, as well as semi-empirical data. A comparison between the three can be made on their use of theory and what experimental data they are based upon. Table 2.1 shows this comparison.

Assumptions	Nikolsky	Bailey	Slaymaker
Satisfies power equation	$\star$	$\star$	$\star$
Thrust based on rotor C_T	$\star$	$\star$	
Thrust based on average blade c_l			$\star$
RPM based on λ	$\star$	$\star$	
RPM based on vertical descent equilibrium			$\star$
Tip losses included		$\star$	
Blade twist assumption	Any function	Linear	None
Based on Fig. 2-8	$\star$	$\star$	$\star$
Based on Princeton flair tests			$\star$
Models transient behavior			$\star$

Table 2.1: Comparison between vertical flight algorithms.[4][18][22]

2.4 Forward Flight Performance

Another beneficial quality of the autogyro is that in forward flight, there is a decrease in the descent speed. In terms of airdrop, this means that the payload can be delivered from further away with a slower impact speed. Obviously, there are limits to both how fast an unpowered system can fly, and how slow it can be made to descend.

Predicting the forward flight performance of an autogyro system is similar to predicting its vertical flight performance. However, in forward flight there are more variables to deal with.

In vertical descent, the rotor itself is level with the horizon. This means an equilibrium solution can be obtained by basically setting thrust equal to weight. However in forward flight, the autogyro must not only be in vertical equilibrium, but also horizontal equilibrium. Thus, the horizontal component of the thrust produced must equal the horizontal components of the body and rotor drag. This means that the rotor cannot remain level with the horizon, but instead must be slightly pitched forward in the direction of flight. Although this complicates matters slightly, the horizontal equilibrium condition allows for adding an extra variable to the equation, and that variable can chosen to be the rotor pitch.

With rotor pitch, θ_R, and RPM set as variables, the power equation and the equilibrium conditions must be solved to determine the trim conditions. For this problem Bailey's Tables become extremely useful. The tables are designed to be used at various tip-speed ratios, μ. The tip-speed ratio is defined as:

$$\mu = \frac{V cos(\alpha_R)}{\Omega R} \tag{2.16}$$

Similar to the relationship between inflow ratio and descent rate, the tip-speed ratio describes the relationship between the forward speed of the rotorcraft and the velocity of its rotor tips. The tip-speed ratio is a limiting factor in the accuracy of performance predictions, as forward flight theory loses accuracy for $\mu < 0.1$ and $\mu > 0.5$.[11] In the case of autogyros, the tip-speed ratio will rarely ever reach 0.5. However, the range from vertical flight, $\mu = 0$, to $\mu = 0.1$ is definitely within the flight regime and must be accounted for.

With a lack of accurate theory in this range, predictions are made on a "connect the points" type basis. That is, performance predictions are made at $\mu = 0$ and $\mu > 0.1$. Then the gap is "filled in" to provide a complete set of data. Using forward flight theory at a tip-speed ratio of zero will cause an error in the predicted rate of descent. Likewise, using vertical descent theory at tip-speed ratios greater than zero will also overestimate the rate of descent.

The low-tip speed ratio gap is due to the fact that in this range the rotor is either

power limited or stall limited.[15] If the rotor is power limited, it must descend more quickly to reach equilibrium, and if it is stall limited it must increase its RPM to break out of the stall, which also requires an increase in descent rate. The power limitations can be predicted as they were for vertical flight. However once the rotor is stalled, conventional momentum theory becomes irrelevant. Thus, the "bridging" theory is used.

As stated earlier, two of the the benefits of using an auotgyro system for airdrop are its vertical descent capabilities and the reduction of descent speed in forward flight, and valid theory exist in both of the regimes. The only area of concern is the "bridging" theory. Due to the fact that that there is no real advantage gained by operating in this regime, it appears that most flight time spent at low tip-speed ratios would simply be a transition from vertical descent to forward flight or vice versa. This type of operation cannot be analyzed by trim conditions anyway. Thus, there is not a significant gain in being able to determine the exact performance in this state.

Chapter 3

Experimental Setup

In order to validate the theoretical predictions, it is necessary to collect experimental data from an environment similar to that experienced during airdrop. Initial testing will use model helicopter rotors. This means the experimental setup would need to be capable of supporting a 4' diameter rotor in flows varying from 0 ft/s to 25 ft/s. With these constraints in mind, three options were initially available.

The first was the Wright Brothers Wind Tunnel (WBWT) located at MIT. The WBWT had a suitable test section area and velocity, but unfortunately had two significant problems. One, like most wind tunnels, the WBWT produces horizontal flow. Although gravitational forces are not a significant factor during full rotation, they do have a considerable effect on the start-up. Thus, a vertical wind tunnel would better reproduce the air drop environment. The other major problem was test time required. Due to both scheduling issues and cost, the WBWT was not a feasible option for the large number of tests that needed to be performed.

The second option was to perform actual air drops. However, due to a lack of experience in deploying autogyros, it was determined that a more controlled environment should initially be used. Obviously, at some point actual airdrop tests will need to be made, but only after a adequate knowledge of the deployment sequence has been gained in a more controlled environment.

Eliminating options one and two, led to option three: build a vertical wind tunnel. Thus, Draper Laboratory is now equipped with the *Draper Vertical Wind Tunnel*.

3.1 Vertical Wind Tunnel Design

The three goals set for the *Draper Vertical Wind Tunnel* (VWT) were: to achieve the required performance parameters, be built in a cost effective manner, and maintain OSHA safety standards. Once it was proven that all three could be achieved construction was approved.

3.1.1 Basic Tunnel Characteristics

The two main parameters around which the VWT was designed were test section area and flow velocity. Since most of the tests would be run using model helicopter rotors, the test area was set to have a 4' diameter, allowing tests to be run on most model helicopter blades. The initial prediction of deployment flight speed was in the 10 to 25 ft/s range. Therefore the tunnel was only required to produce flow velocities up to 25 ft/s.

Basic wind tunnel design involves three sections. A fan or blower to create the flow, a smoothing section, and the test section.[6] With vertical tunnels, there also must be a section which turns the flow upwards, unless of course the tunnel is set up in a room with extremely high ceilings, and the entire tunnel can be constructed vertically.

Figure 3-1 shows the initial design of the VWT. The fan is shown in red, flow smoothing is in green, and the test section. in this case a nozzle, is blue. At this point in the tunnel design, it was determined that a centrifugal blower would be used. This is because the centrifugal blower produces the required flow rate at the lowest cost.

Also, due to the fact that flow losses are proportional to flow velocity, a large plenum is used to slow down the flow while it was "turned" vertically. Within the plenum a perforated, "smoothing" sheet is also used to further improve the flow quality. After the plenum, a converging nozzle brings the flow back up to the required speed. The opening of the nozzle is shaped octagonally due to the fact that structurally a perfectly circular nozzle would have been difficult to construct.

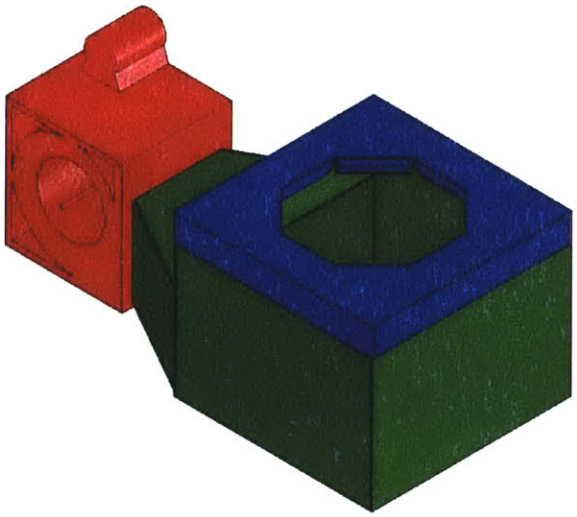

Figure 3-1: Wind Tunnel CAD Design

Fig. 3-2 shows a sideview of the VWT. The various sections of the tunnel are color coded, and the important geometric properties are labeled. These properties are the nozzle area, A_{noz}, the plenum area, A_{plen}, the turn area, A_{turn}, and the blower exit area, A_{blower}. Also Fig. 3-2 shows how the test article is mounted directly above the nozzle, in the air flow.

From these preliminary design points, the next step was to calculate flow losses through the tunnel sections in order to choose the appropriate blower and drive package.

3.1.2 Flow Losses

Flow losses and pressure drops are directly proportional to the dynamic pressure, $\frac{1}{2}\rho V^2$, in a particular section of the tunnel. This fact implies that the greatest flow losses occur at the highest tunnel velocities. Thus, the critical design point will in

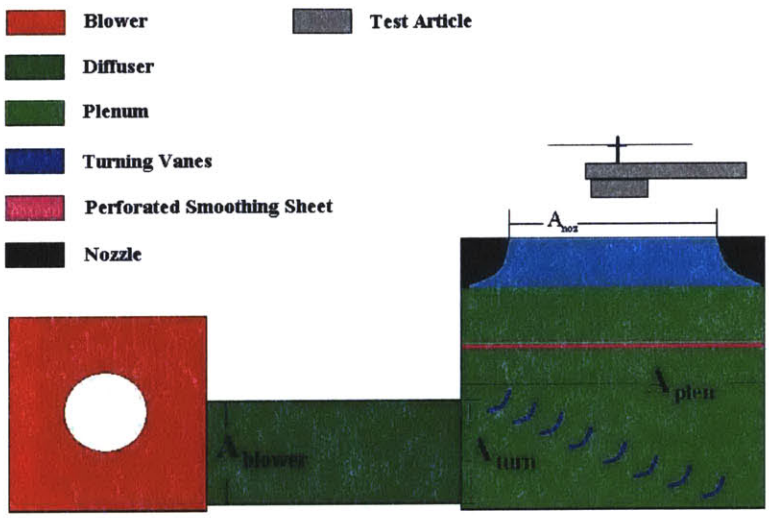

Figure 3-2: Wind Tunnel Side View

this case come at a test section velocity of 25 ft/s.

Choosing a motor/blower combination to power the tunnel requires that the entire system be capable of delivering the correct velocities at a back pressure determined by the flow losses in the tunnel. The losses in the tunnel can be calculated by determining the given loss for each section of the tunnel and then summing the losses. These losses occur in the diffuser, the turning section, across the perforated flow smoothing sheet, and in the nozzle itself. The two equations used to determine the losses are the mass flow equation for incompressible flow, Eqn. (3.1), and Bernoulli's equation, Eqn. (3.2).

$$A_1 V_1 = A_2 V_2 \tag{3.1}$$

$$\Delta p = \frac{1}{2}\rho(V_2^2 - V_1^2) \tag{3.2}$$

Where A is the area of a section, V is the air velocity through that section, ρ is

the air density, and the subscript determines the section.

To calculate the losses it is easiest to start from the end, in this case the nozzle. This means that Eqns. (3.1) and (3.2) must be used to calculate the losses between the plenum and the nozzle. Rearranging and substituting the two equations gives:

$$V_{plen} = \frac{A_{noz}}{A_{plen}} V_{noz} \tag{3.3}$$

$$\Delta p = \frac{1}{2}\rho\left(1 - \left(\frac{A_{noz}}{A_{plen}}\right)^2\right) V_{noz}^2 \tag{3.4}$$

The next set of losses to be calculated comes from the flow crossing the perforated sheet. Here the sheet porosity, R, is considered to be the open portion of the perforated sheet.

$$V_{sheet} = \frac{A_{noz}}{R A_{plen}} V_{noz} \tag{3.5}$$

$$\Delta p = \frac{1}{2}\rho\left(1 - \frac{1}{R^2}\right)\left(\frac{A_{noz}}{A_{plen}}\right)^2 V_{noz}^2 \tag{3.6}$$

Notice that the flow losses across the sheet are still dependent on the flow velocity at the nozzle and the ratio of nozzle area to plenum area. This is because the losses are dependent upon the velocity through each section, and the velocities are dependent upon the desired test section velocity, in this case V_{noz}.

In the turning and diffuser sections of the tunnel, losses can be determined from the same principles used to calculate losses in ducting systems. The American Society of Heating, Refrigerating, and Air-Conditioning Engineers provides a set of tables for the flow losses through various duct sections. Each loss is calculated by multiplying the loss coefficient, C_0, by the dynamic pressure at the section entrance. The loss coefficients can be found in Ch. 33 of Ref. [20], and are dependent upon section geometry.

For the turning section the flow properties are:

$$V_{turn} = \frac{A_{noz}}{A_{turn}} V_{noz} \tag{3.7}$$

$$\Delta p = \frac{1}{2}\rho\Big(\frac{A_{noz}}{A_{turn}}V_{noz}\Big)^2 C_{0_{turn}} \tag{3.8}$$

Likewise in the diffuser, the flow properties are:

$$V_{turn} = \frac{A_{noz}}{A_{blower}}V_{noz} \tag{3.9}$$

$$\Delta p = \frac{1}{2}\rho\Big(\frac{A_{noz}}{A_{blower}}V_{noz}\Big)^2 C_{0_{diff}} \tag{3.10}$$

Finally, summing up the losses across all four sections of the tunnel gives.

$$\Delta p = \frac{1}{2}\rho\Big(1-\Big(\frac{A_{noz}}{A_{plen}}\Big)^2\Big)\Big(1-\frac{1}{R^2}\Big)\Big(\frac{A_{noz}^3}{A_{plen}A_{turn}A_{blower}}\Big)^2 C_{0_{turn}}C_{0_{diff}}V_{noz}^2 \tag{3.11}$$

This pressure loss term defines the blower, and thus tunnel performance. It is dependent upon the given area of each section of the tunnel, the geometry of the diffuser and turning section, and the porosity of the smoothing sheet. In the case of the Draper VWT, the nozzle size was preset, limits on available space defined the plenum and diffuser sizes, and the blower exit size was determined by the manufacturer. That left only the smoothing sheet porosity and the turning section geometry as variables.

At that point it was determined that turning vanes would be used to minimize flow losses. The vanes could potentially provide a 500% increase in turning performance over just a flat corner.[20] This efficiency was realized in $C_{0_{turn}}$.

That left only the perforated sheet porosity as an open variable. Fig. 3-3 was obtained by plotting nozzle velocity against pressure drop for various porosities, and overlaying the plot with the blower performance curves for various motors.

The desired test section velocity was 25 ft/s. Fig. 3-3 shows that a 5 HP motor could provide about 24 ft/s for smoothing sheet porosities of 40% or less. A variable speed motor drive was already in the room and was used to control the motor at speeds below 24 ft/s. This design was deemed to be adequate and construction began with the final tunnel parameters set as:

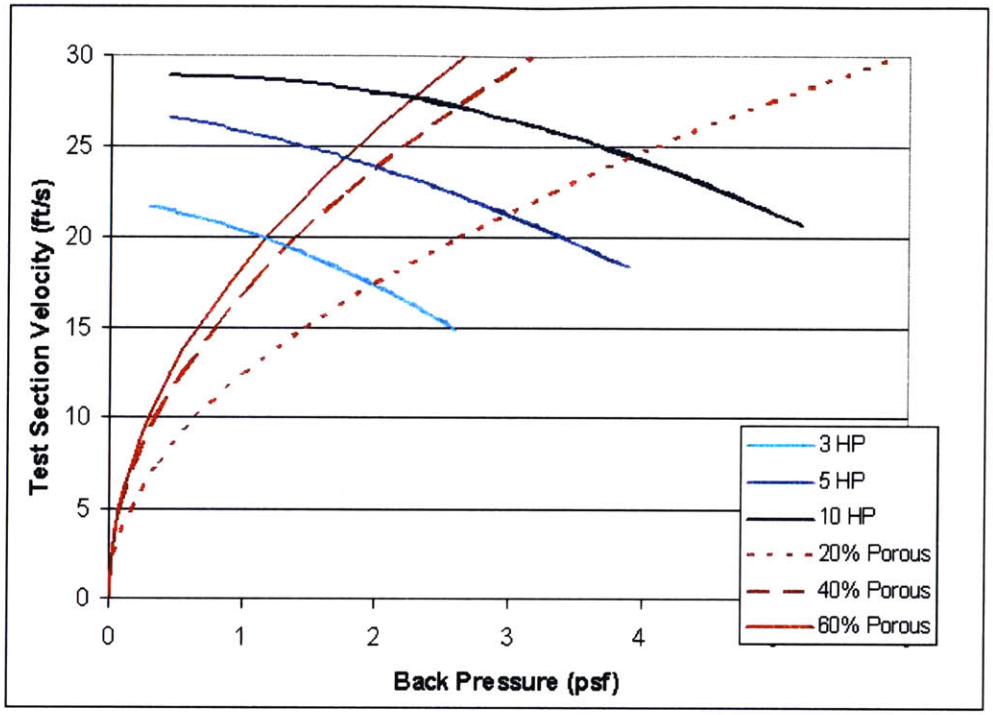

Figure 3-3: Test Section Velocity vs. Back Pressure

- A_{noz} : $13.28 ft^2$
- A_{plen} : $36 ft^2$
- A_{turn} : $15.63 ft^2$
- A_{blower} : $6.78 ft^2$
- $R(Porosity)$: 40 %
- $C_{0_{turn}}$: 0.15
- $C_{0_{diff}}$: 0.22

Fig. 3-4 shows the VWT as an almost finished product. The only feature added after this picture was taken is a plexiglass safety shield around the test section.

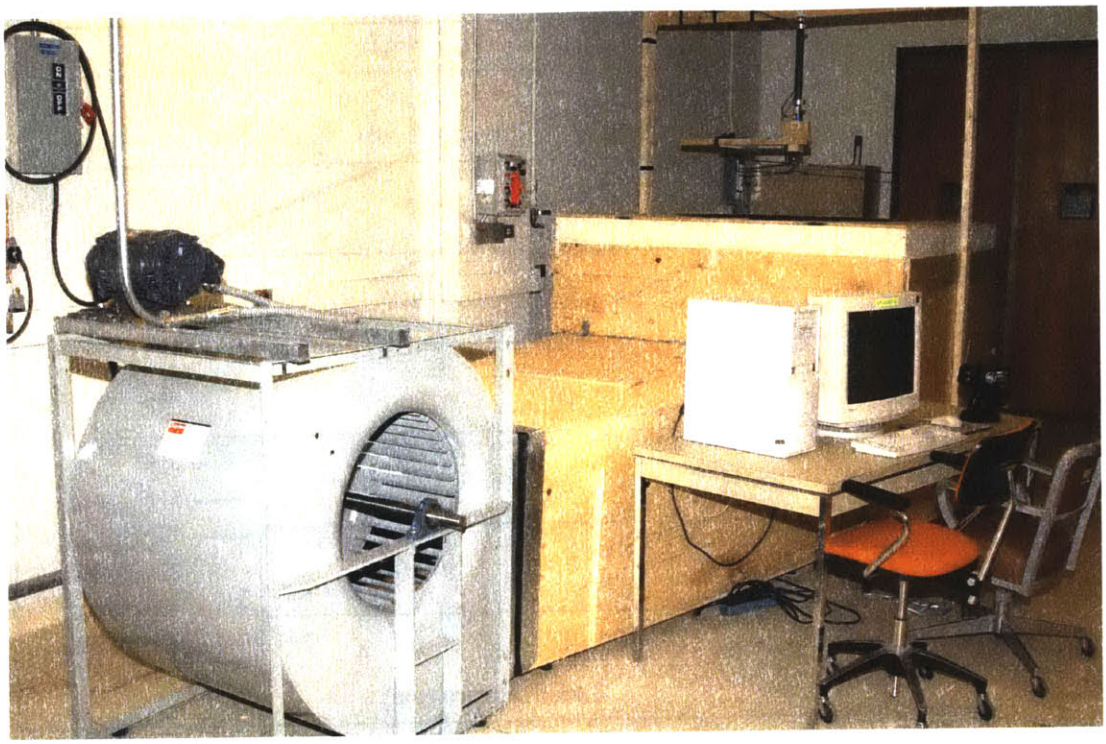

Figure 3-4: Draper Vertical Wind Tunnel

3.1.3 Instrumentation

Initially, the VWT was only supposed to provide airflow to simulate the deployment environment. However, during the design process it was determined that some type of instrumentation to measure lift and drag produced by the rotor, as well as rotor RPM, would be beneficial.

For the force calculations, a JR3 6-DOF load cell was borrowed from a previous project at Draper. The JR3 can measure up to 30 lbs of vertical load, 15 lbs of horizontal load, and 30 in-lbs of torque on all three axis. With a sample rate of 8 KHz, and the capability of directly interfacing with MATLAB, the JR3 system was an ideal fit for the project.[13]

For the RPM counter, a much simpler instrument was needed. Fig. 3-5 shows the basic design of the counter circuitry. Three magnets were attached to the rotor hub equally spaced apart. When they came within 0.1" of the magnetic switch in the

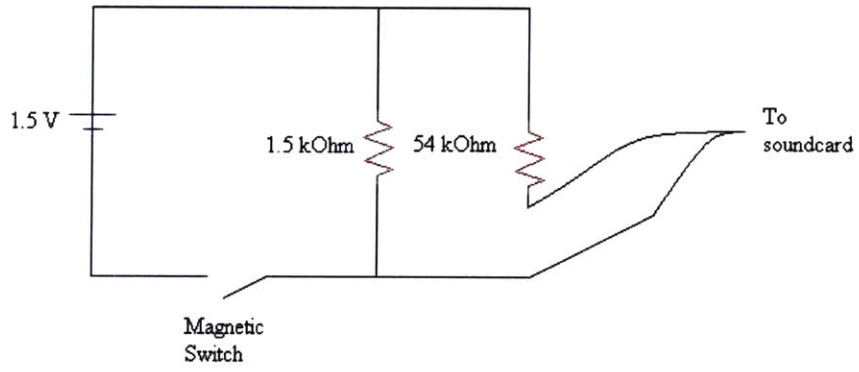

Figure 3-5: RPM Counter Circuit Diagram

RPM counter, they closed the circuit and sent a low current ping to the computer soundcard. MATLAB's Data Acquisition Toolbox [17] was then used to count these pings and create an RPM vs. Time plot from the raw data.

The code used to collect the load and RPM data is contained in the Digital Appendix. RPMcollect.m was used to collect the data. RPManalyze.m and Tanalyze.m were used to analyze the data.

3.1.4 Wind Tunnel Calibration

Once the VWT and instrumentation were functional, tunnel calibration began. The calibration focused on two goals: improving the overall flow quality in the test section and determining an accurate test section velocity for a given controller setting.

The first step in accomplishing both goals was to determine the initial flow properties in the tunnel. This was done by creating an 8x8 grid of 6" squares, which would be used to segment the test section. As Fig. 3-6 shows, the three squares in each corner were outside of the test section and were not used. This left 52 segments which could be used to analyze the flow.

To initially assess the flow quality the tunnel was run at controller settings of 10,

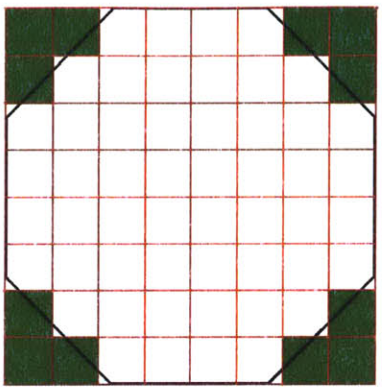

Figure 3-6: Calibration grid

20, and 30 Hz. At each setting an Extech Vane Anemometer, accurate to $\frac{1}{6}$ ft/s, was used to measure the flow velocity over each segment of the calibration grid. [10] The data was then entered into MATLAB to create a flow quality plot. Each velocity was normalized over the average velocity of the entire test section to better compare various speeds.

To determine whether or not a smoothing sheet would be required in the tunnel, the initial calibration data was taken with no sheet. As can be seen in Fig. 3-7, the velocity across the test section was extremely variable.

The top of the plot represents the portion of the test section farthest away from the blower. Thus, the flow enters the plenum from the bottom of the plot, and then turns upward (out of the page). Fig. 3-7 shows that the highest test section velocities are occurring at the back of the test section. This infers that, without a smoothing sheet, the flow is not being redirected by the plenum and turning vanes as well as anticipated. The velocity across the test section varies by over 60%.

To correct these initial problems, the flow smoothing sheet was added. With the addition, the normalized tunnel flow characteristics improved as can be seen in Fig. 3-8.

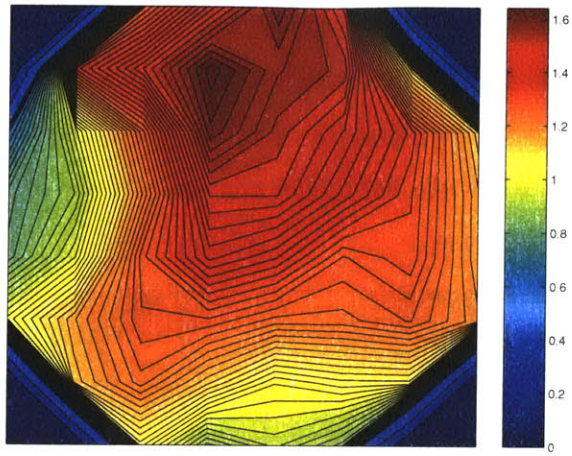

Figure 3-7: Initial test section flow quality (view looking down on test section).

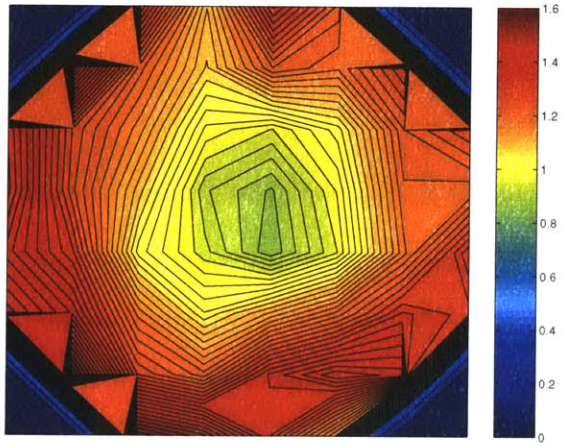

Figure 3-8: Test section flow quality with smoothing sheet

With the addition of the perforated sheet, the velocity profile is now nearly radially symmetric. Considering the experiments that will take place in the tunnel, namely rotor testing, this is a large improvement over the flow in Fig. 3-7, whose velocity would vary over the blades throughout a revolution. Also, the overall difference in flow velocity across the test section is now down to about 40%. The major fault with the flow profile is now the velocity decrease in the center of the test section.

In order to remove the velocity dip, holes were drilled in the center of the smoothing sheet to minimize the losses incurred there. Theoretically, this would speed up

the flow in that portion of the test section and improve the overall flow quality. Fig. 3-9 shows the results of this improvement.

With this modified smoothing sheet, the total velocity difference across the test section is now approximately 20%. This was considered a sufficient flow quality, and the tunnel was put into use.

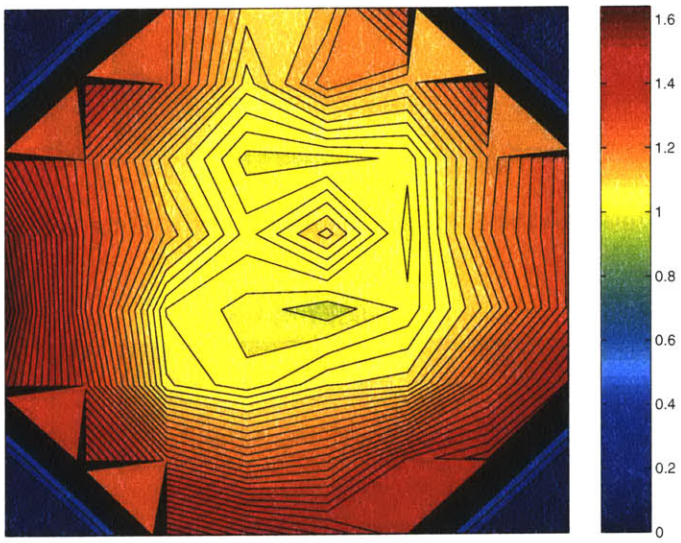

Figure 3-9: Final test section flow quality

Unfortunately, the corrections made to the flow quality did not make enough improvement to accurately determine the test section velocity during experimental runs. Most wind tunnels are designed to have less than 10% blockage, which is defined as the ratio between the test article area to the total test section area.[6] In this case:

$$Blockage = \frac{Rotor\ disk\ area}{Nozzle\ area} \tag{3.12}$$

The VWT has almost 90% blockage. This amount of blockage is off the charts for theoretical wind tunnel calibration methods. Thus, it was decided that the final velocity calibration would be done experimentally.

Theoretically in ideal autorotation, there is zero resultant velocity through the rotor disk.[14] Taking advantage of this fact, it was proposed that the tunnel could be calibrated by replacing the rotor with a flat disk. The disk would have many properties

similar to the rotor, as well as one large advantage, a known drag coefficient. In *Fluid Dynamic Drag*[12], Hoerner determines that for reasonable Reynolds numbers, the drag coefficient for a flat disk is 1.17. The calibration setup can be seen in Fig. 3-10, where h is the distance between the nozzle and the disk.

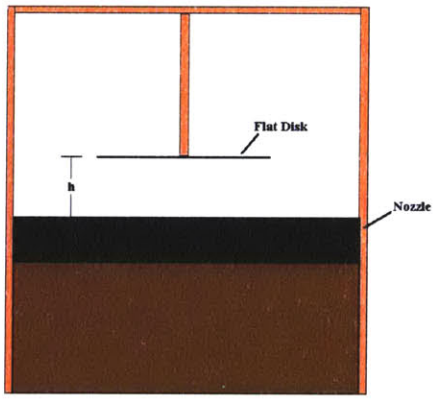

Figure 3-10: Calibration setup.

During the initial calibration, the average tunnel velocities were calculated for an unobstructed test section. Using these values and Hoerner's drag coefficient, a correction factor could be determined which would eliminate the effects of blockage on the thrust and RPM data. In the following derivation: the subscript t represents the true value, and *initial* is the value based on the initial tunnel calibration.

$$T_{initial} = c_{d_{initial}} \frac{1}{2} \rho V_{initial}^2 \pi R^2 \tag{3.13}$$

$$T_t = c_{d_t} \frac{1}{2} \rho V_t^2 \pi R^2 \tag{3.14}$$

The JR3 load cell has been accurately calibrated. Thus, its thrust, $T_{initial}$, output is taken as the true thrust.

$$T_{initial} = T_t \tag{3.15}$$

$$c_{d_{initial}} \frac{1}{2} \rho V_{initial}^2 \pi R^2 = c_{d_t} \frac{1}{2} \rho V_t^2 \pi R^2 \tag{3.16}$$

$$V_t = V_{initial}\sqrt{\frac{c_{d_{initial}}}{c_{d_t}}} \tag{3.17}$$

And $c_{d_t} = 1.17$:

$$V_t = V_{initial}(0.9245\sqrt{c_{d_{initial}}}) \tag{3.18}$$

The accuracy of this method of calibration relies on the resultant velocity through the rotor. Based on ideal autorotation, where no flow passes through the rotor, the flat disk model is completely accurate. However, in actual autorotation the inflow ratio is never zero. Thus, the accuracy of the correction factor will depend on how close the rotor is to ideal autorotation.

During calibration, the flat disk was placed at various heights above the nozzle, and $c_{d_{initial}}$ was calculated based on Eqn. (3.13). The results for the velocity correction factor, $0.9245\sqrt{c_{d_{initial}}}$ can be seen in Fig. 3-11.

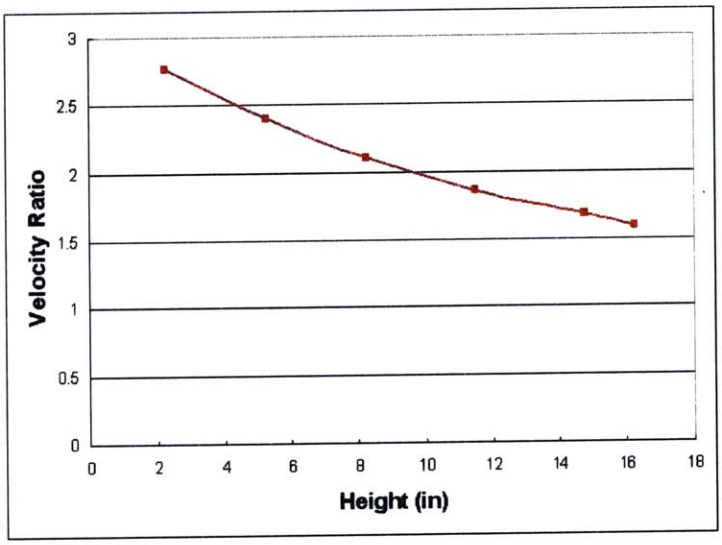

Figure 3-11: Correction factor vs. Height above nozzle

Fig. 3-11 shows that as the test article is moved further away from the nozzle, the velocity correction factor decreases. With such a high blockage value, this may be a simple mass flow problem. As the test article is moved downstream from the nozzle, i.e. upward, it becomes easier for the tunnel jet to get around the outside of the rotor disk. Also as h increases, the correction factor appears to asymptotically approach

a value of one. Theoretically with an open test section such as this, at an infinite distance the blockage should not affect the test section velocity, and the correction factor should be one. The data appears to agree with this. However, due to the fact that positions over 16" from the nozzle couldn't be tested, this cannot be conclusively proven.

While the flat disk can be used to model the blockage caused by the autogyro, it does not model another correction which needs to be made, bearing friction. The rotor is attached to the sting balance with a bearing designed by *Master Airscrew*. [19] This bearing works extremely well when there is no load placed on the rotor. However, as the rotor is loaded, the bearing friction tends to increase. This in turn decreases the RPM and thrust.

The simplest way to eliminate this effect comes from the RPM curve. RPM linearly increases with descent velocity. When the tunnel velocity equals zero, RPM should also equal zero. The collected RPM data is extremely linear, but it shows zero RPM at approximately 1.2 ft/s. Simply subtracting out the 1.2 ft/s value leaves a RPM curve, which is both linear and passes through the origin. This correction also causes the thrust curve to pass through the origin as theory predicts.

Taking into account both the blockage and friction corrections, the test section velocity models the descent velocity by the following relation.

$$V_{descent} = ((0.9245\sqrt{c_{d_{initial}}})V_{initial} - 1.2)ft/s \tag{3.19}$$

Although these corrections fix the tunnel inaccuracies in a simple manner, it is left to Ch. 5 to determine the how they relate to the theoretical performance predictions.

3.2 Autogyro Design

After the VWT was built and calibrated the test articles were built. In order to perform a parametric analysis on the different possible rotor configurations, a sting mounted instrumentation system was needed, and for the simulated deployment sequence, an actual test vehicle was built.

3.2.1 Test Models

In order to take advantage of the JR3 load cell and the RPM sensor, it was necessary to mount various rotor configurations to a sting system. This mounting system needed to be capable of providing accelerating torque to the rotor and varying the rotor angle of attack.

The accelerating torque was provided by 3/8" surgical tubing, which was used as a high-elasticity rubber band. The tubing was doubled up and attached to kevlar line. This line was then wrapped around the shaft of the rotor. The blades were held in place by a controllable arm. Once the tunnel reached a predetermined speed, the arm was released, and the surgical tubing accelerated the rotor. Once fully unwrapped, the kevlar line would release from the shaft and was stored inside a fiberglass shield. Fig. 3-12 shows the surgical tubing hanging out of the shield on the left side of the model. Because of the small rotor moment of inertia, this system could accelerate the rotor to up over 500 RPM.

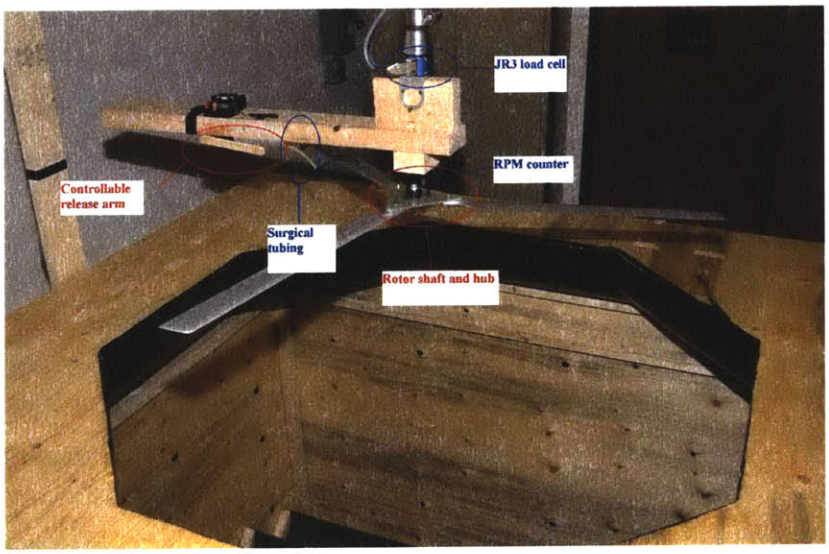

Figure 3-12: Sting mounted model

The rotor angle of attack was controlled by a system of wedges. Fig. 3-12 shows the model with a 90^o angle of attack wedge. The wedge is the block of wood attached to the JR3 load cell, the blue puck. To vary the angle of attack, other wedges varying

from 60^o to 90^o could be inserted.

Once the mounted model was designed and tested, the more complicated deployment model was constructed. During the actual deployment, a drag parachute will be used to slow down the system's descent rate. The connection to this drag chute was modeled by suspending the deployment model from two lines attached to the wind tunnel cross bar. A swivel was then used to allow the autogyro system complete rotational freedom.

When starting the sting mounted model, the necessary counter torque to spin-up the rotor was provided by the sting and in turn the wind tunnel itself. Due to the fact that the deployment model is attached to a swivel, which does not transfer torque, the counter torque for its prerotation was provided by the body of the autogyro. Torquing both the rotor and fuselage with the surgical tubing caused them to rotate in opposite directions. In order to dampen out the rotation of the body, a vertical tail was attached to the deployment model. The deployment model can be viewed in the Digital Appendix by opening any of the video files.

3.2.2 Airfoils

Over the course of the project, four different airfoils were used: a NACA 0012, a Clark-Y, a SG6042, and a airfoil of unknown section provided by the Autogyro Company of Arizona. The airfoil characteristics can be seen in Table 3.1. Drag data are not included do to the fact that at low Reynold's numbers, both the profile and induced drag coefficients vary greatly at different airspeeds.

Airfoil	Span (in)	Chord (in)	Aspect Ratio	c_{l_α} $(/^o)$
NACA 0012	24.0	2.00	12	0.106
Clark-Y	21.25	1.73	12.5	0.101
SG6042	20.5	1.38	14.9	0.109
Arizona Autogyro	25	2.00	12.5	n/a

Table 3.1: Airfoil characteristics [1] [21]

The NACA 0012, Clark-Y, and Arizona Autogyro airfoils were purchased as finished products. The SG6042 cross-section was bought, and the airfoils were finished

at Draper Laboratory. The NACA 0012 was fiberglass, the Clark-Y was bass wood, and the SG6042 and Arizona Autogyro blades were balsa wood.

3.2.3 Hub Design

The hub design was based on that used by the Autogyro Company of Arizona (ACA).[19] The hub obtained from ACA was constructed of a 1/8" thick G10 fiberglass and triangular in shape to support three blades. However, the 1/8" G10 was not rigid enough. Due in part to the nature of the sting mounted system, at high test section velocities the rotor coning angle would cause blade strikes on the surgical tubing shield. Thus, a second triangular hub was made using 3/16" G10. The extra rigidity in the 3/16" solved the coning issue.

The finished triangular hub can be seen in Fig. 3-13. Notice the magnets attached to the hub, which are used to close the RPM circuit.

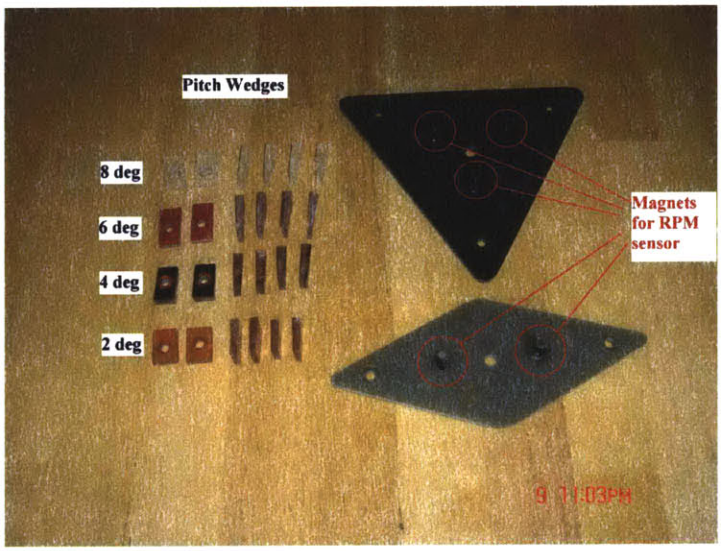

Figure 3-13: Rotor hubs and pitch wedges.

A two-bladed hub was also designed. Instead of a triangle, the two-bladed hub was shaped like a diamond. Aside from that difference, the two hubs were constructed in the same method. The two-bladed hub can also be seen in Fig. 3-13.

Possibly the most important aspect of the hub design was the blade pitch control. On most rotorcraft, pitch control is accomplished by collective. However, in an effort to prove the simplicity and cost efficiency of our design, it was determined that testing and initial prototyping would be accomplished with a fixed blade pitch. Obviously, the aim of the project being to determine the effects of blade pitch, a single fixed pitch would not suffice, and without collective it is difficult to change blade pitch. This presented a significant problem.

The solution to this problem was to use pitch wedges. The concept, as illustrated in Fig 3-14, is to flatten the airfoil section where it is attached to the hub. This will be called "blade smoothing." Then the bolt which connects the blade to the hub is run through the wedges and a securing nut before reaching the hub. In this manner, the relative blade pitch can be controlled to within the accuracy of the wedges.

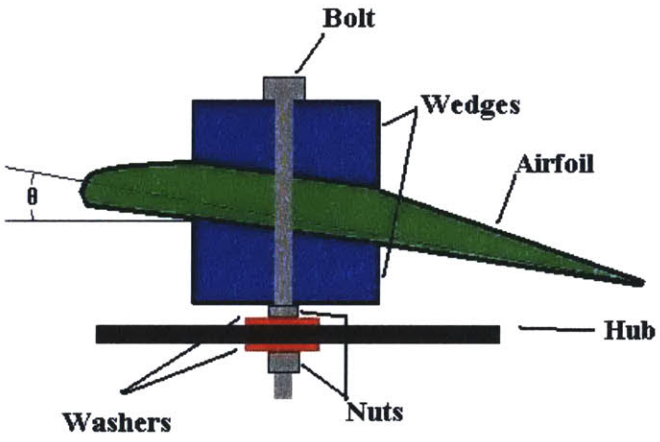

Figure 3-14: Pitch wedge design. Note: not drawn to scale.

During the blade smoothing process it is possible to achieve the same pitch on similar blades. However, it is extremely difficult to smooth the blades to an exact pitch with a high degree of accuracy. At the angles of attack in which autogyros operate, a pitch error as small as two degrees can often double the lift generated by the rotor. Therefore, even though the blades were all given the same initial pitches,

the exact value of this pitch was unknown. The difference between the published zero lift angle of attack and the given blade's zero lift angle of attack is to be determined through testing. Thus, without correction the pitch wedges only give "relative" pitch control.

The pitch wedges were molded from epoxy. The appropriate angles were created by raising one end of an 8' plank the correct height, placing a flat mold on the plank, and allowing gravity to fill the mold with epoxy. Using the 8' plank allowed control of the wedge pitch to within 0.1^o.

Chapter 4

Theoretical Performance Evaluation

Utilizing the theory laid out in Ch.2, performance predictions can be made to discover the effects of varying the rotor parameters. This evaluation will explore the two regimes of vertical descent and forward flight. Within each of these areas, focus will be placed on descent rates and rotor RPM. The final section will analyze the benefits of adding a collective flare during landing to decrease touchdown speed.

Unless otherwise noted, all analysis will be done on the generic system described in A.1.

4.1 Vertical Descent

In order to accurately predict the performance of the autogyro in vertical descent, it is necessary to understand the relationship between the resultant velocity and descent speed. Thus, the first analysis done in the vertical flight regime looked at the differences in results obtained between the Glauert and Georgia Tech resultant velocity curves as described in Section 2.3.1. Once the correct relationship is chosen, a parametric analysis can be performed to predict the flight performance of the system. This analysis focused on utilizing the various theories of Nikolsky, Bailey, and Slaymaker, to predict the effect of blade pitch and rotor solidity on the descent speed

and RPM.

4.1.1 Analysis of the Resultant Velocity Curves

As seen in Fig. 2-8 on page 39, the Glauert resultant velocity curve and the Georgia Tech resultant velocity curves vary significantly. The lower branch of the curves model behavior in the vortex ring state, while the upper branches model flow in the windmill brake state. From the simple knowledge that the vortex ring state is turbulent and less predictable than the windmill brake state, the Georgia Tech curve at first appears to be more reasonable.

Fig.4-1 shows the descent speeds obtained through the Bailey and Nikolsky methods using both resultant velocity curves.

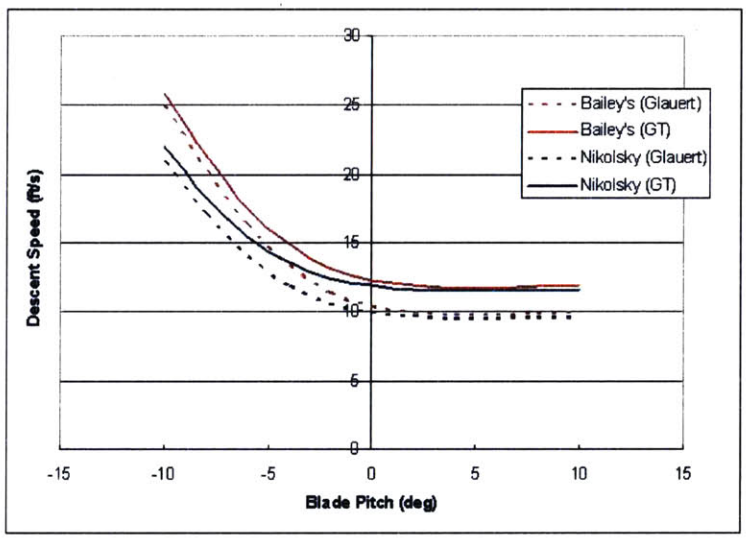

Figure 4-1: Descent velocity comparison

At low blade pitches the algorithm used, original Nikolsky or Bailey's, is more influential in determining the behavior of the descent velocity. This can be seen at negative blade pitches where the two Bailey's curves are similar and the two Nikolsky curves are similar. However, as blade pitch increases, the algorithm becomes less important, and instead the semi-empirical data used, Glauert or Georgia Tech (GT),

becomes more influential. At high pitch values, the two curves which used the GT data are similar, and the two curves which utilize the Glauert data are similar.

This result is most likely due to the nature of the Glauert and GT curves. At low values of blade pitch, the descent velocity is high and the rotor is operating in the windmill brake state. In this state the experimentally collected data are similar. However, as blade pitch is increased and descent velocity is decreased, the rotor begins to enter the vortex ring state. At this point, the Glauert and GT curves display much different behavior. As the goal of this project is focused on operating at low descent speeds, the curve which gives better performance estimates in this low descent speed range will be used henceforth.

In order to determine exactly which curve, Glauert or GT, produces more accurate results, the rotor drag coefficients for Fig. 4-1 were plotted in Fig. 4-2.

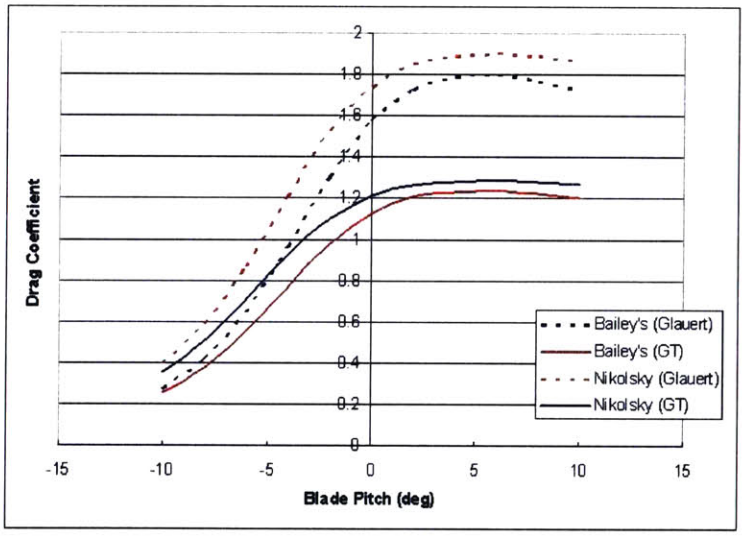

Figure 4-2: Drag coefficient comparison

Generally, rotor drag coefficients, c_{d_R} are approximately 1.2.[16] From Fig. 4-2, it can be seen that at positive blade pitch angles the GT curves do in fact predict drag coefficients of 1.2. The Glauert curves reach drag coefficients over 1.8. This value is extremely high and is not realistic. This implies that the GT resultant velocity curve is more accurate, and thus will be used for all further analysis.

4.1.2 Effects of Blade Pitch

Earlier it was mentioned that blade pitch has a significant impact on the flight performance of autogyros. If the blade pitch is set too high, the blade will stall and the rotor will not be able to maintain an autorotative state. If the pitch is too low, a large degradation will occur in the thrust obtained. Similar to start-up considerations, the the correct choice for pitch lies somewhere in the middle, providing solid performance without the danger of blade stall.

Vertical Descent Speed

All three theories utilized to predict the system descent speed contain the same flaw. They do not account for blade stall. This flaw lies in two of the assumptions used to develop the performance equations:

- 1 The blade drag coefficient can be described by either a constant term or a parabolic curve.
- 2 The blade lift curve slope is linear.

As far as drag is concerned, the constant drag term never comes close to modeling the sudden drag spike seen as stall occurs. Although the parabolic drag polar does a better job, at stall the drag increase is even more drastic than what is modeled by the quadratic curve. Lift on the other hand tends to decrease after stall. On some airfoils there is a sharp drop-off, while on others the post-stall characteristics are relatively benign. However, no airfoil sees a continued linear increase in lift beyond stall as is modeled by the second assumption.

Thus, due to the inability of the algorithms to model the stall condition, the performance analysis will be stopped prior to the blade reaching its stall angle of attack. The first performance analysis can be seen in Fig. 4-3. The three curves display the vertical descent predictions of the various algorithms for the generic system.

All three algorithms predict similar results. It can be seen that at negative blade pitches, an increase in blade pitch will decrease descent speed. However as the blade

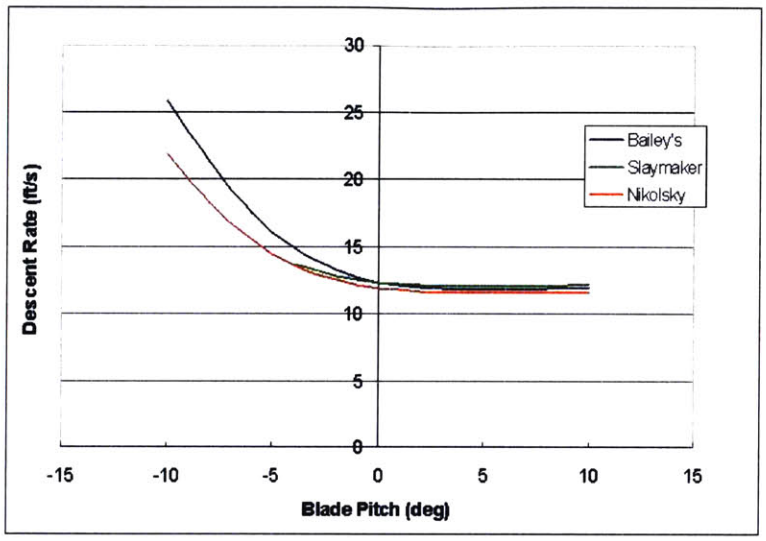

Figure 4-3: Equilibrium descent rates for various blade pitches.

pitch reaches 2^o, the working state, this trend stops as predicted, and the rotor performance tends to remain constant for changes further increases in pitch.

Fig. 4-4 shows the same data plotted as rotor drag coefficients. Similar to the generally accepted value, the normal working state drag coefficients are all in the range of 1.2.

Rotor RPM

The blade pitch setting will also effect the rotor RPM. Having a good estimate for RPM is important for a number of reasons. Probably the most important is structural failure. While the blades are spinning, they create a centrifugal force on the rotor hinge proportional to their mass and angular velocity. Thus, if the RPM become exceedingly large, the hinge will break and the system will fall apart.

Another reason RPM should be calculated is to estimate the kinetic energy stored in the rotor. Any energy stored in rotor in the form of rotational energy can be used in flight as a pseudo-power source. For instance, the flare maneuver is performed by increasing the blade pitch during flight. This maneuver provides a decrease in descent speed and can even cause a climb if the situation is right. The outcome of the flare is

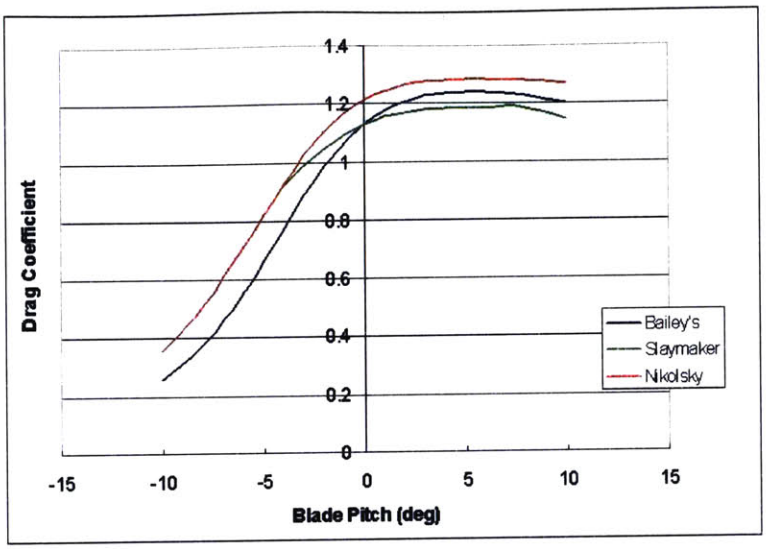

Figure 4-4: C_{D_R} versus blade pitch

dependent on the rotor moment of inertia and its initial RPM. An increase in initial RPM will increase the rotational energy stored in the rotor. This energy can then be transferred to the entire system to slow its descent rate during the flare. Fig. 4-5 shows the effect of blade pitch on the rotor RPM.

The original algorithms, Nikolsky and Bailey's, give similar results. However, the Slaymaker algorithm predicts much higher RPMs. The difference in results is found in the methods used. The first two methods solve for equilibrium inflow conditions, and then use the inflow value and the blade pitch angle to solve for RPM. The Slaymaker algorithm instead chooses an average blade lift coefficient and uses this value to solve for RPM. Unlike the drag coefficient, there is no general rule of thumb that can be used to validate RPM results. Thus, wind tunnel testing will be used to decide which algorithm is more accurate. These results will be shown in Section 5.1.3.

Fig. 4-5 also shows that as the blade pitch is increased, RPM decreases. In the working state of the rotor, this concept is fairly intuitive. If the blade pitch is increased, thus increasing angle of attack and the blade drag coefficient, the blade will slow down to reach a new equilibrium inflow angle based on Eqn. (2.3) from page 26. Theoretically there is a blade pitch for maximum RPM. To find this maximum

value, Fig. 4-5 was extended to $\theta = -40^o$ in Fig. 4-6.

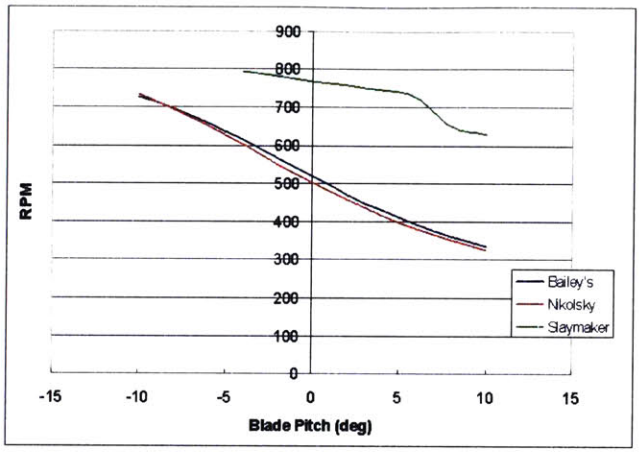

Figure 4-5: RPM versus blade pitch

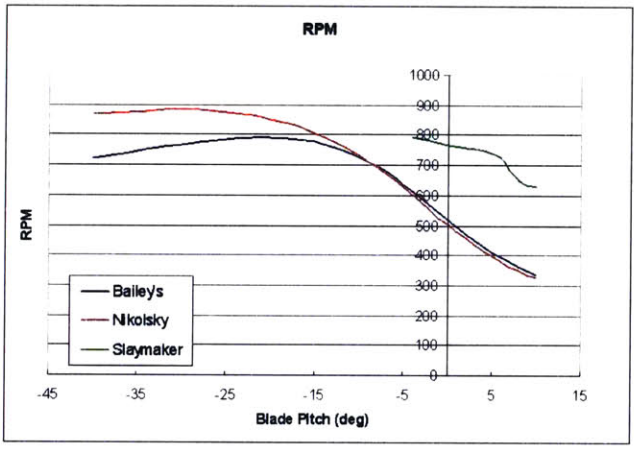

Figure 4-6: Extended RPM versus blade pitch

Unfortunately, because the average lift coefficient data was collected experimentally and only extends to zero degrees blade pitch, the Slaymaker theory cannot be used in this analysis. Using only the Nikolsky and Bailey algorithms it can be seen that in vertical descent the maximum RPM occurs at a significantly negative pitch. The Nikolsky data predicts that the maximum RPM will occur at -30^o, while Bailey's theory gives a maximum at -20^o.

It is interesting to note that these low pitch values are over 20^o outside of the working state of the rotor and actually are more indicative of pitch settings used in turbines than autogyros. Although the maximum RPM takes place outside the working state of the rotor, its value is not entirely lost. Depending on the efficiency of the energy transfer during flare, it may be more beneficial to enter the flare maneuver with a low blade pitch, high RPM, and high descent rate, as opposed to a high blade pitch, low RPM, and low descent rate. This problem will be examined in Section 4.3.

4.1.3 Effects of Rotor Solidity

Another important factor in determining rotor performance is rotor solidity. For a constant chord blade, rotor solidity is calculated as:

$$\sigma = \frac{total\ blade\ area}{total\ rotor\ area} = \frac{bc}{\pi R} \tag{4.1}$$

where b represents the number of blades, and R is the rotor radius. Solidity can be varied by changing either the blade chord or the number of blades.

Vertical Descent Speed

In this project, rotor solidity was varied by changing the number of blades on the rotor. Due to the nature of the airdrop program, only two and three blade configurations were studied. This limitation is not based on performance, but rather space constraints placed on airdrop packages. Two and three bladed rotors can be folded into a much smaller package than a four bladed rotor. When competing against parafoils, which can be packed very tightly, the space issue becomes a major concern.

Packing constraints aside, Fig. 4-7 shows the effect of blade count on the descent speed.

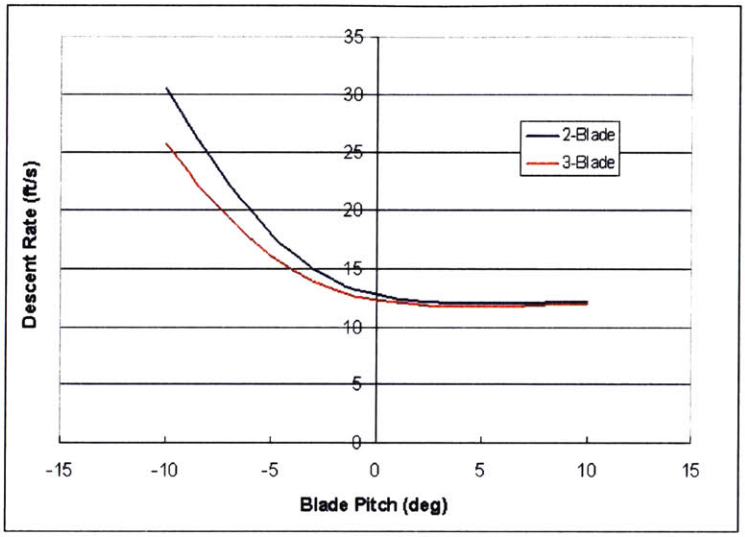

Figure 4-7: Effect of rotor solidity on descent speed.

Outside of the working state of the rotor, in this case $\theta < 2^o$, the two-bladed system descends more quickly than the three-bladed system. However, in the working state, both systems descend at similar rates. Fig. 4-8 shows the drag coefficients for the two configurations.

The same trend occurs in drag coefficient as descent speed. Outside the working state, the three-bladed rotor performs better, but once in the working state c_{d_R} is roughly the same. This behavior should not be surprising as the original heuristic predicts that $c_{d_R} \approx 1.2$ and never mentions any caveats about solidity effects. This fact does, however, imply that the extra lift produced must come from somewhere, and that somewhere is the RPM.

Rotor RPM

Aerodynamic forces are dependent on three main criteria: characteristic area, air velocity, and an aerodynamic coefficient. If one is varied, the others must also change in order to maintain equilibrium. When the number of blades on a rotor, the charac-

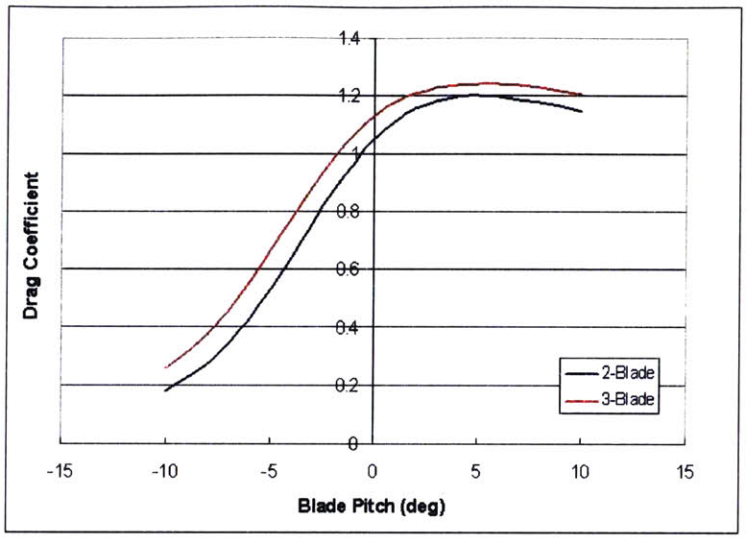

Figure 4-8: Effect of solidity on drag coefficient.

teristic area, is decreased, the RPM must increase to increase the air velocity over the airfoil. Fig. 4-9 illustrates the change in RPM caused by switching from a three-blade to a two-bladed rotor.

Both rotors display the same trend. However, the two-bladed rotor's RPM is approximately 25% greater than that of the three-bladed rotor over the range of pitches analyzed. Similar to pitch effects, the effects of rotor solidity can be used to increase or decrease the rotor RPM. If a low RPM is required for structural concerns, the three-bladed rotor should be chosen. If instead, a high equilibrium RPM is necessary, the two-bladed rotor would be the correct choice.

4.2 Forward Flight

Forward flight analysis was focused in three main areas: accuracy of results obtained from bridging theory, as well as the effects of blade pitch and rotor solidity. Unlike vertical descent, forward flight analysis must calculate performance in two dimensions. Combining vertical descent predictions with forward flight speeds can give lift-to-drag ratios, the system's range, and landing performance criteria, as well as the previously

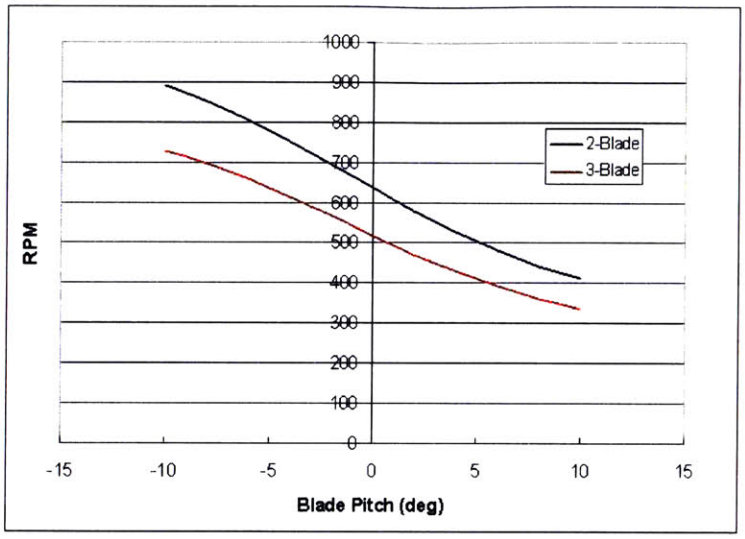

Figure 4-9: Effect of solidity on rotor RPM.

analyzed descent rate and RPM. For the purpose of this analysis the body drag component of the test vehicle will be assumed to be 0.3 ft^2.

4.2.1 Analysis of the Bridging Theory

In autorotation analysis, it is understood that there are two sets of theories: one for vertical descent and another for high speed forward flight. Because the two theories contain different assumptions, using vertical flight theory to predict forward flight performance, and vice versa, will produce errors in the results.

Currently simulations are being designed to model the autogyro's behavior, and eventually these models will be used to design a controller for flight tests. Because the flight tests will cover the full range of the flight envelope, it is important to understand the error incurred by using both methods across the envelope. If the error is small enough, then it is possible that one of the theories could be used throughout the entire flight envelope. If, however, the error in both theories proves to be too large, a bridging theory will be used during the transitional period. Fig. 4-10 shows the descent rate prediction over the full flight envelope for the three theories with blade pitch set at 0^o.

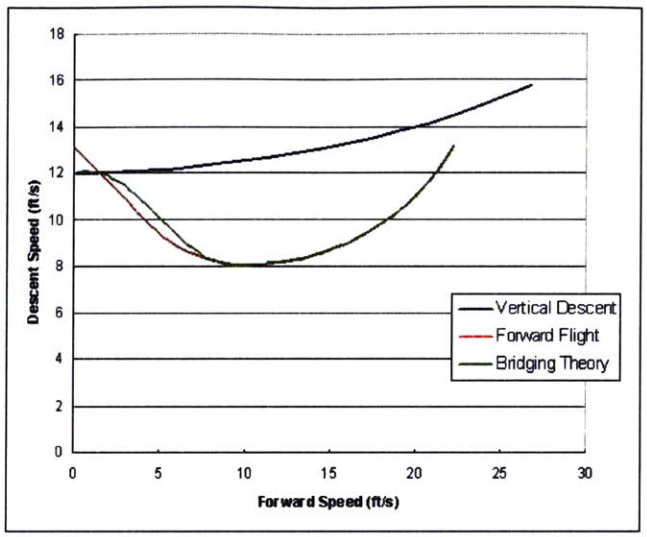

Figure 4-10: Error incurred when using one theory across entire envelope.

The green curve in Fig. 4-10 is a combination between vertical descent and high forward speed equilibrium theory. At zero forward speed, the descent speed is obtained purely from vertical descent value theory. Between flight speeds of 0 and approximately 10 ft/s, the descent speed is a ratio between the vertical descent theory and the forward flight theory. Beyond 10 ft/s only forward flight theory is used. This curve is accurate across the entire flight envelope and can be used to determine the error incurred if only one theory is used for all forward flight speeds.

It is quite apparent that the vertical descent theory produces poor results for any forward speed much past 5 ft/s. This fact quickly eliminates any chance of using the vertical descent theory across the entire flight regime.

On the other hand, the forward flight theory does not contain a very significant error in pure vertical descent. At zero forward speed, there is only an error of approximately 10%. Depending on the type of analysis being performed, this error may be acceptable. In order to determine if the error remains constant for various rotor configurations, Fig. 4-11 shows the effect of pitch and rotor solidity on the accuracy of the forward flight theory in vertical descent.

At low values of pitch, vertical descent theory predicts higher descent rates than

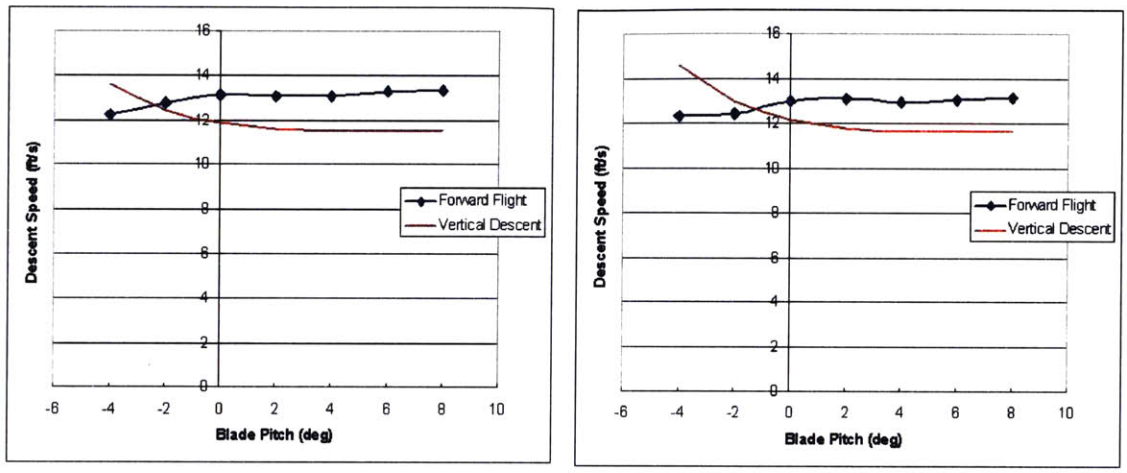

Figure 4-11: Effects of blade pitch and rotor solidity on prediction error.

the forward flight theory and the difference between the two theories varies. However, in the working state of the rotor, the error appears to stay constant with forward flight theory predicting descent rates approximately 10% greater than the vertical descent theory. That being said, it appears that forward flight predictions algorithms can be used across the entire flight envelope, as long as a 10% error is acceptable.

Comparing plots (a) and (b) of Fig. 4-11 shows the effects of rotor solidity on the error. Both plots display the same trends and have similar magnitudes. Thus, it can be said that rotor solidity has very little effect on the accuracy of using forward flight theory to predict vertical descent rates.

4.2.2 Effects of Blade Pitch

In vertical descent, it was shown that increasing blade pitch will improve rotor performance, i.e. decrease descent rate, until stall is reached. In forward flight, overall system performance is not solely dependent on the minimum descent speed attained, but is also based on factors such as forward speed and lift-to-drag ratio, L/D.

Increasing the rotor pitch increases the drag produced by the rotor. Thus, a pitch setting that might be desirable in vertical descent, may cut back on the system's

range in forward flight. Fig. 4-12 shows system performance for three pitch settings.

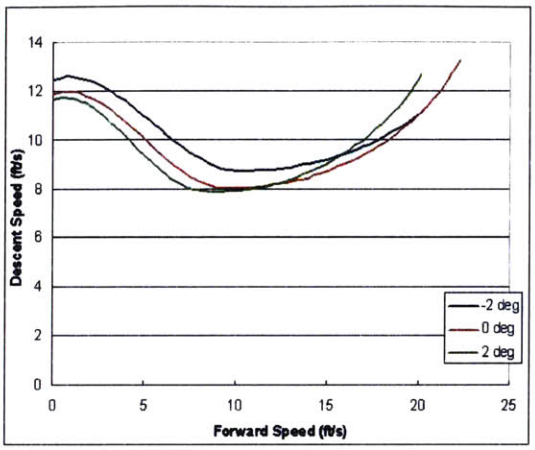

Figure 4-12: Effects of blade pitch on forward flight performance; 3 blades.

As shown, increasing the blade pitch not only decreases the descent rate, but also decreases the forward speed achieved at a given descent rate. Depending on the intended use of the system, the pitch setting could be used to optimize performance in forward flight or vertical descent. Fig. 4-13 shows the effect of blade pitch on the lift-to-drag ratio of the system.

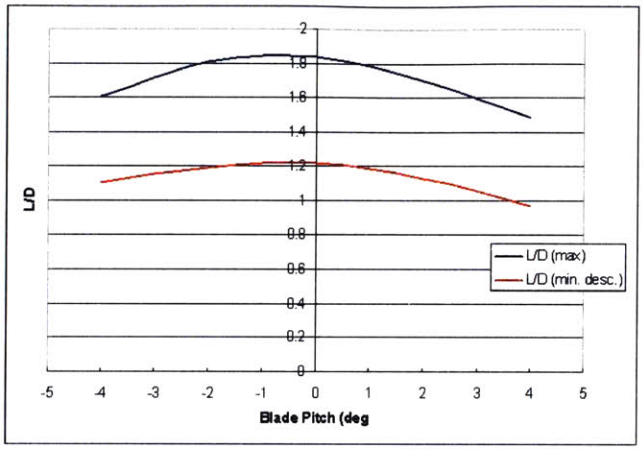

Figure 4-13: Effects of blade pitch on L/D ratio; 3 blades.

In Fig. 4-13, the maximum lift-to-drag ratio occurs at a pitch setting of -0.5°. This value is slightly below 2°, which was deemed the working state of the rotor in Section 4.1.3. This shows that increasing blade pitch into the working state causes a decrease in L/D_{max}. A L/D ratio below two is considered poor for most aircraft. However, these low values are due to the fact that at low Reynolds numbers, there is a significant increase in parasitic drag. On a larger scale vehicle, the maximum lift-to-drag ratio would be between four and five.

If the maximum range is not an issue, and instead the minimum descent speed is desired, the L/D ratios all decrease by approximately 50%. This means that the system will descend more slowly, but at a steeper angle to the ground. For landing purposes, this type of approach may provide both softer touchdowns and shorter roll distances, similar to the effect of lowering flaps on an aircraft.

4.2.3 Effects of Rotor Solidity

In vertical descent it was shown that rotor solidity had very little impact on the descent speed if the rotor was operating in the working state. The same holds true for the forward flight analysis. Fig. 4-14 shows the a plot of descent speed versus forward speed for both a two bladed and three bladed system.

At low forward speeds, the three bladed rotor descends more slowly than the

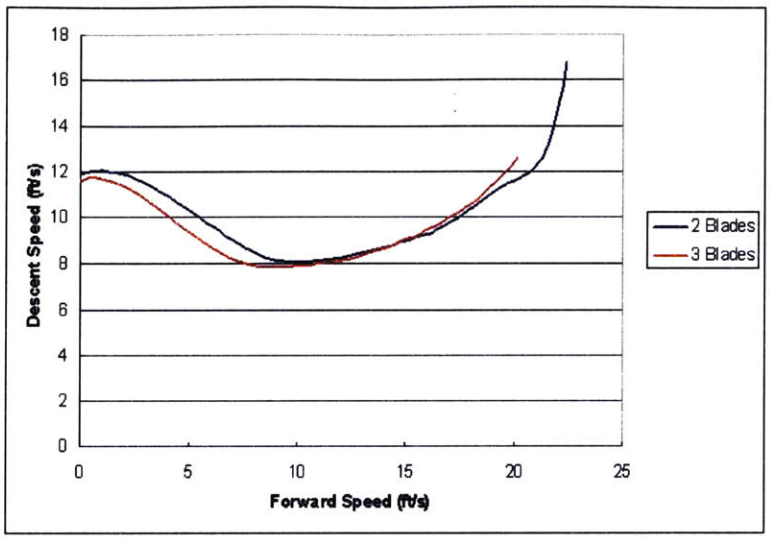

Figure 4-14: Effects of rotor solidity on descent rate.

two bladed rotor. The difference is not significant, and seems to be similar to the variations in descent speed seen in pure vertical descent. As flight speed increases, it appears that this disparity in the descent speeds is erased.

Fig. 4-14 also shows that similar to vertical descent the three bladed system has a slightly slower minimum descent speed. For the three bladed system, this overall minimum descent speed occurs at a slower forward speed than the minimum descent speed for the two bladed system. This fact will have an influence on the L/D values of the two systems. Fig. 4-15 shows both the maximum and minimum descent L/D ratios for both systems.

There is little difference in the maximum lift-to-drag ratio of the two systems. This could be expected, since maximum L/D occurs at higher forward speeds where both systems show similar performance. On the other hand, the L/D ratios at minimum descent speeds show a larger difference, with the two bladed system being about 10% greater. At the minimum descent velocity, this implies that the two bladed system will have a shallower descent angle. However, Fig. 4-14 shows that it will also have a higher descent speed. As far as the terminal phase of flight is concerned, this leads to harder landings and longer roll-out distances.

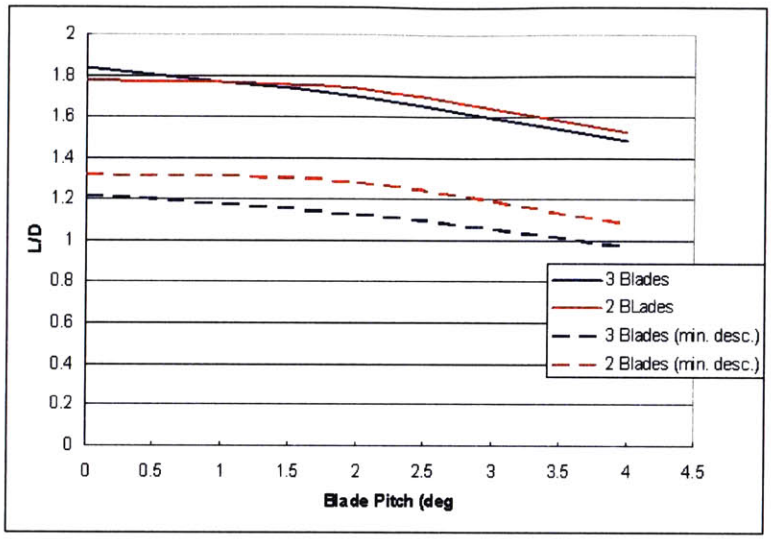

Figure 4-15: Effects of rotor solidity on L/D ratios.

Although it is the inferior system in terms of landing performance, the two bladed system does have some advantages. The higher minimum descent L/D ratio means that if the system is forced to loiter, i.e. fly the minimum descent speed, it will have a greater range.

After analyzing the effects of rotor solidity on forward flight performance, it appears that similar to vertical descent, the three bladed rotor is the better choice. It provides lower minimum descent speeds, as well as better landing performance, two criteria which are important in designing airdrop systems.

4.3 Collective Flare

Choosing whether or not to design a rotor with collective is a matter of cost versus performance. During most of the flight, a set blade pitch does not infringe too heavily on the performance of the autogyro. However, as stated earlier, the start-up procedure could be improved by including collective in the design. Another stage of flight which would benefit from collective is the landing.

When aircraft land, the pilot must pitch-up the nose of the aircraft to decrease

the vertical speed at touchdown. This procedure known as flaring is also used by helicopter pilots, but to a different extent. Not only do helicopter pilots pitch-up the aircraft, they also increase the pitch of the rotor blades. Doing this takes kinetic energy from the rotation of the rotor, and adds it to the downward airflow, thus slowing the descent speed.

Flaring is also possible in autorotation. However, due to the fact that there is no engine producing torque, the amount of energy available is limited. During flares in autorotation, the descent speed is decrease for a short amount of time by using what kinetic energy is available in the rotor. As the energy is transferred to the surrounding air, the rotor RPM also slows down. At a certain RPM, the energy exchange no longer benefits the system and the descent speed begins to increase.

At this point the system must either have landed, or the blades must again be pitched down to re-initiate stable autorotation. If neither of these occurs, the result will be total rotor stall and an uncontrolled descent. With an autogyro this energy exchange maneuver is extremely difficult, since it must be performed at the exact instant to be useful.

Because the flare maneuver is an energy transfer process with rotational energy being traded for kinetic "lifting" energy, its performance is dependent upon the amount of energy stored in the rotor. Rotational energy is calculated as $I_r\Omega^2$, where I_r is the rotor's moment of inertia. Thus, the rotational energy can be increased by increasing blade RPM or increasing the I_r.

As shown earlier, RPM can be increased by either pitching the blades down to the setting for maximum RPM or decreasing the number of blades. Fig. 4-16 shows the variation of descent rate over time during a flare maneuver for various initial RPM.

The solid blue line represents the baseline three bladed rotor operating at a blade pitch of zero degrees. The other two configurations show the effect of increasing RPM through either decreasing the initial blade pitch, blue dashed line, or decreasing the number of blades, solid red line.

The baseline configuration decreases the descent speed from 13 ft/s to 2.5 ft/s. The low pitch three bladed rotor enters the maneuver with a higher RPM, i.e. rotational

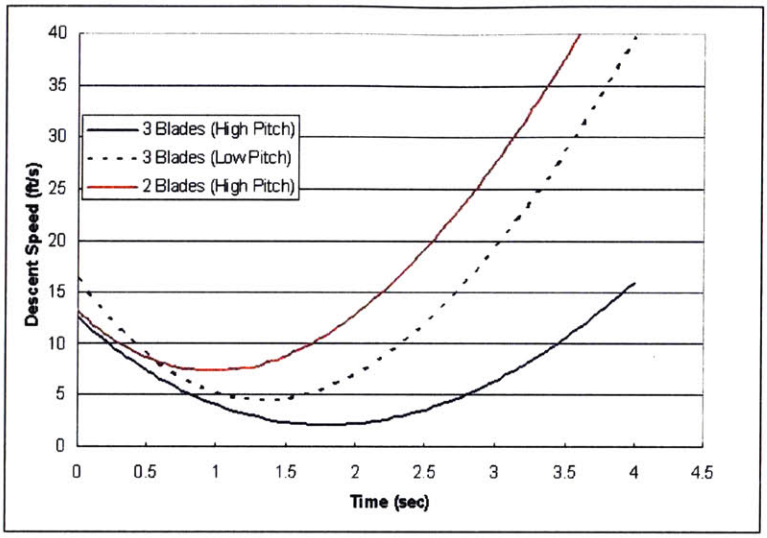

Figure 4-16: Effect of initial RPM on flare performance.

energy, but also a faster descent speed. Fig. 4-16 shows that the increased rotational energy is not enough to improve the overall flare performance. The two bladed rotor also enters with a high RPM, but a similar descent speed. However, it does not perform as well as the baseline configuration either. This is because having one less blade reduces the moment of inertia of the rotor, which in turn decreases the rotational energy.

If increasing RPM is eliminated as a method of increasing the rotational energy, the only other option is to increase the moment of inertia. Fig. 4-17 shows the effect of increasing the rotor moment of inertia on flare performance.

The dashed lines in Fig. 4-17 represent the effect of doubling the rotor moment of inertia. This modification causes a significant improvement in flare performance and can be easily made by adding weights to the tips of each blade. With the increased moment of inertia the three bladed rotor can actually achieve a climb for short durations of time. Also the total duration of flare is increased allowing more room for error while the maneuver is being performed.

Although it may be a difficult maneuver to autonomously control, the flare can be seen to dramatically improve the touchdown speed of the autogyro. For airdropping

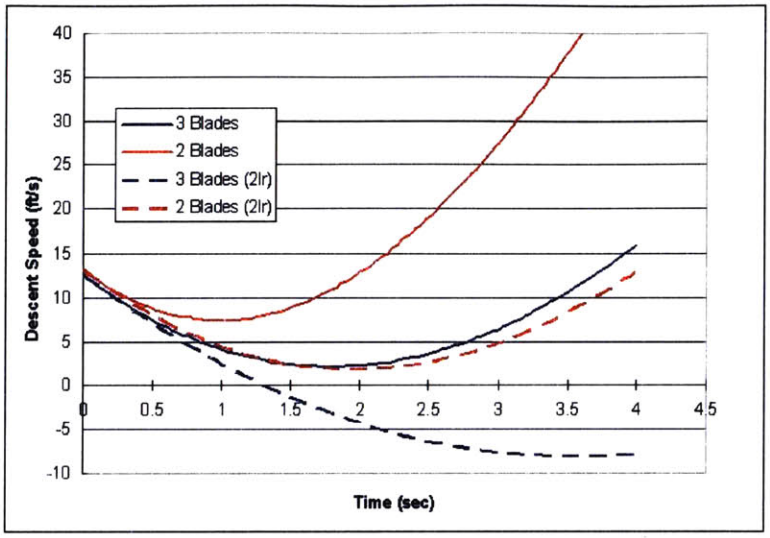

Figure 4-17: Effect of I_r on flare performance.

hard payloads, such as food and munitions, this extra soft landing may be unnecessary. However for sensitive items, like sensor packages, the soft landing could be an enormous benefit.

4.4 Final Thoughts on Theoretical Predictions

Throughout the theoretical analysis, one major issue continually emerged, which limited the accuracy of the predictions. This problem was the effect of the blade drag coefficient.

In the basic power equation, Eqn. (2.8) on page 36, the component of power lost due to profile drag is based on a constant drag coefficient. This simplification is false because it ignores the fact that the drag coefficient varies with blade angle-of-attack, α_B. As α_B increases beyond the zero-lift angle-of-attack, the drag coefficient increases parabolically up to stall. Ignoring this fact creates a significant error in profile losses when the blade is operating at high angles of attack.

In the more advanced theories, a parabolic curve is used to model the increase in drag coefficient due to angle-of-attack. These results are more accurate, but another

error emerges. Using the parabolic drag polar requires that the drag act parabolically. Fig. 2-6 on page 33 shows the drag polar's variation at low Reynolds numbers. The drag coefficient at low values of Reynolds number, up to 100,000, cannot be modeled by a quadratic. In this range, the drag coefficient becomes dependent on parameters such as skin smoothness and flow quality and behaves erratically. Thus, it is difficult to predict, let alone fit with a smooth curve.

Because Reynolds number is proportional to total velocity, every section of the blade has a different Reynolds number. In vertical descent, this varies due to radial position. While in forward flight the Reynolds number also varies due to the angular position of the blade. Analyzing model helicopter scale rotors can be a difficult task due to Reynolds number. Fortunately however, as Reynolds number increases, the drag polar becomes much more predictable. Thus, in the analysis of larger scale rotors, this would not be as significant of a problem.

All of this analysis was done using MATLAB. The computer code for the performance predictions can be found on the digital appendix. A.2 contains a complete listing of available programs with a brief description of each.

[This page intentionally left blank.]

Chapter 5

Experimental Results

Having completed the theoretical performance analysis, the focus was shifted to validating those results with data from the Draper Wind Tunnel. The first step in this process was to verify the accuracy of the tunnel. Then thrust and RPM data were collected for various rotor configuration at tunnel speeds ranging from five to fifteen ft/s. During each run, the blade pitch and number of blades were changed. This data was then compared with the theoretical predictions to determine the accuracy of the various theories.

5.1 Raw Data Comparison

Thrust and RPM values were collected for each rotor configuration for at least four values for blade pitch, four values for rotor angle of attack, two rotor solidity configurations, and ten tunnel speed settings. This led to hundreds of test runs in the wind tunnel, and a large amount of raw data. Although every test run was not fully analyzed, for reference all raw data can be found on the digital appendix in the file tests.xls.

Before a parametric analysis can be performed, the accuracy of the raw data must be verified. Remember that in the wind tunnel design, a large amount of effort was placed into determining the quality and velocity of the test section airflow. The final results of that work were to create a blockage correction factor based on the height of

the test article above the nozzle and to eliminate the velocity constant which appeared due to the bearing friction in the system.

5.1.1 Precision of Data Collected

The utility of a data collection system, in this case the wind tunnel, relies on both its accuracy and precision. Accuracy describes how close the data collected is to the true value, while precision describes the repeatability of the results. For instance, if the true temperature for seven days was 80^o, and a certain thermometer read 95^o each day, the thermometer would be precise, but not accurate. If it read between 79^o and 81^o, it would be accurate, but not precise. If it read 80^o everyday, it would be both accurate and precise.

For the purposes of data collection, precision is extremely important. Instruments which are precise, but inaccurate can be corrected after testing to eliminate any bias and achieve results that are both accurate and precise. However, if the instrument is not precise, it is impossible to come up with a correction factor that will always work. Thus it was necessary to determine the precision of the Draper Vertical Wind Tunnel.

Overall, 16 test runs were used to determine the precision of the system. After each of the first eight runs, the rotor was disassembled, and -2^o pitch wedges were randomly selected to be rotated. This simulated the effect of running an entirely new experiment where the pitch wedges may not be have been inserted in the exact same manner. This analysis determined the precision of the sensors, as well as the repeatability of the rotor set-up procedure. During the second eight test runs, the pitch wedges were not rotated. This determined the precision of the sensors alone.

The first precision analysis was performed on the RPM sensor. Fig. 5-1 shows the precision of the RPM values at a blade pitch of -2^o. Fig. 5-1*a* shows the data collected when the pitch wedges were rotated. The red slashes represent the mean value for each tunnel setting, while the blue error bars show one standard deviation. For each tunnel setting, the RPM never showed a deviation greater than 2%. Fig. 5-1*b* shows the same results when the rotor set-up was not varied. As expected, the precision

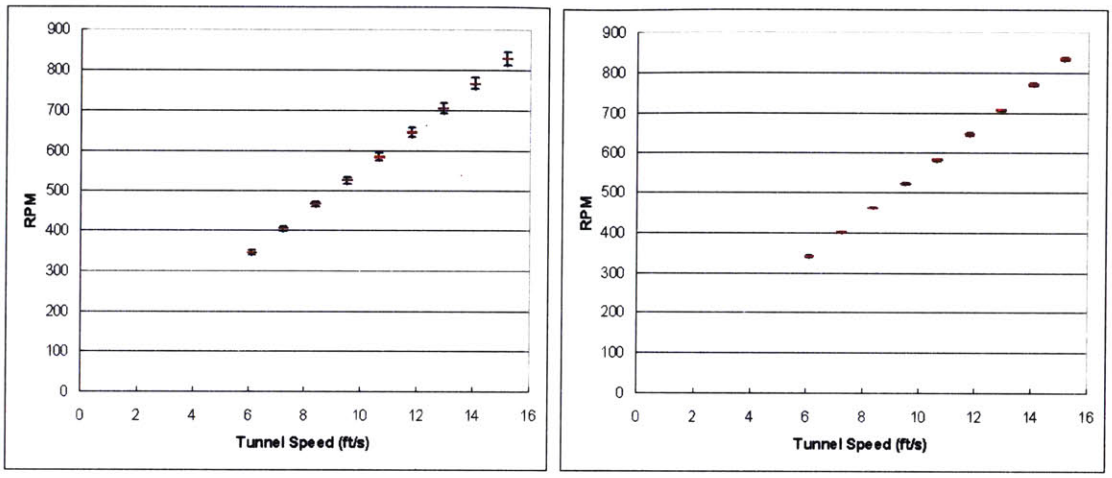

(a) Varying pitch wedges

(b) Fixed pitch wedges

Figure 5-1: Precision of RPM sensor.

was improved for this scenario, and the standard deviation never rose above 0.6% of the mean value. Overall both cases showed that the RPM results are extremely repeatable. Considering the simplicity of the RPM sensor, this was to be expected.

During these same tests, thrust data was collected to evaluate the precision of the JR3 load cell when used in the wind tunnel. Fig. 5-2 shows these results. The average deviation in the thrust data collected tends to be slightly greater than the deviation in RPM data. For the varying pitch case, Fig. 5-2(a), the average deviation is roughly 3%. However, at tunnel settings between 12 and 14 ft/s, the deviation jumps up to 13% of the mean value. A similar phenomenon occurs in the constant pitch wedge case shown in Fig. 5-2(b). The average deviation is 3.5%, yet between 12 and 14 ft/s this value jumps up to 8%.

During the tests runs, it was noticed that the sting itself began to shake at tunnel settings around 12 ft/s. This points to the fact that the sting-rotor setup may reach its natural frequency in the RPM range. While around its natural frequency, the vibrating sting balance puts a widely varying load on the JR3. This may cause the spread in data. Fig. 5-3 shows the percent deviation of the thrust data plotted against the rotor RPM.

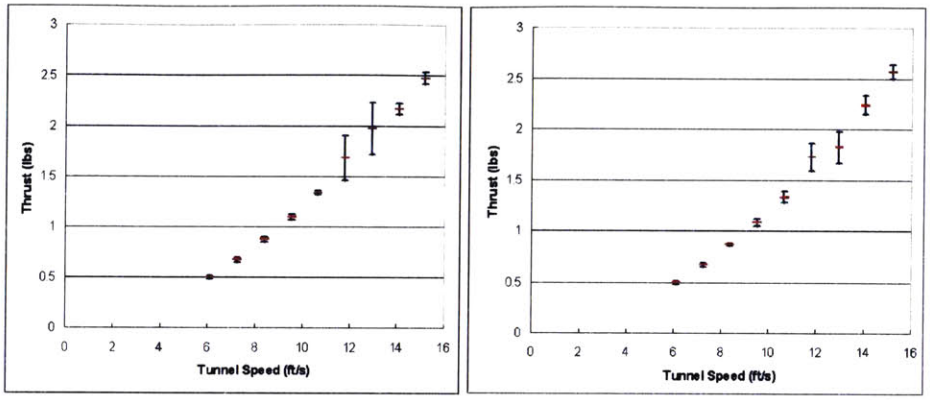

Figure 5-2: Precision of JR3 load cell.

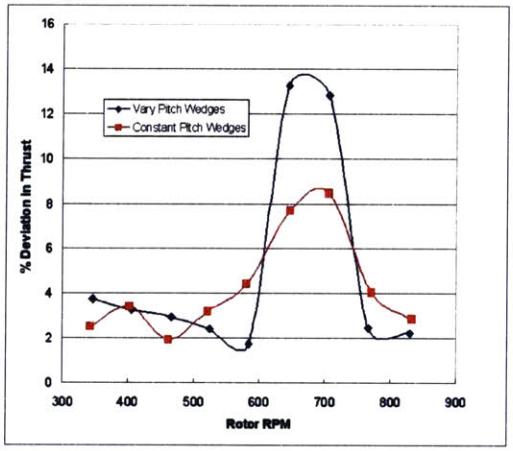

Figure 5-3: % Deviation of Thrust Data.

Fig. 5-3 shows that in both sets of data, the peak error occurs at roughly 700 RPM, or 73 Hz. Even in these worst case scenarios, the percent deviation never exceeds 14%. Fig. 5-4 shows the actual raw data collected during a single test run.

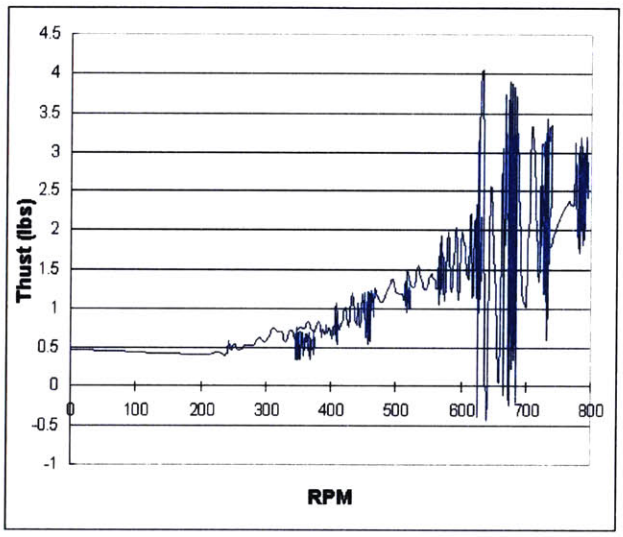

Figure 5-4: Raw data collected from wind tunnel.

From Fig. 5-4 it can be seen that at all RPM values, the collected thrust varies. However, as the rotor exceeds 600 RPM, the thrust values become extremely erratic. As the rotor RPM is increased beyond this point, the collected thrust data begins to show less deviation. The raw data clearly shows that between 600 and 750 RPM there is significant noise in the thrust data. However, when averaged out over time, this noise can be reduced to deviations of less than 15%.

Overall, the sensors provide very precise results. For most of the data collection the data deviates less than 5%. Even in the worst case scenarios, thrust around 700 RPM, the data is still precise to within 14%. This precision will ensure that the correction factors applied to achieve accuracy are applicable to all test runs.

5.1.2 Thrust Produced

System performance relies on the thrust produced to determine factors such as descent speed and lift-to-drag ratios. Thus, the primary goal of the wind tunnel testing was

to determine if the theoretical algorithms predicted an accurate value for thrust. Fig. 5-5 shows the thrust produced for both the two bladed, (a), and three bladed, (b), rotor configurations, as well as the predictions from all three theoretical algorithms. All data is taken with the blade pitch set to -2^o.

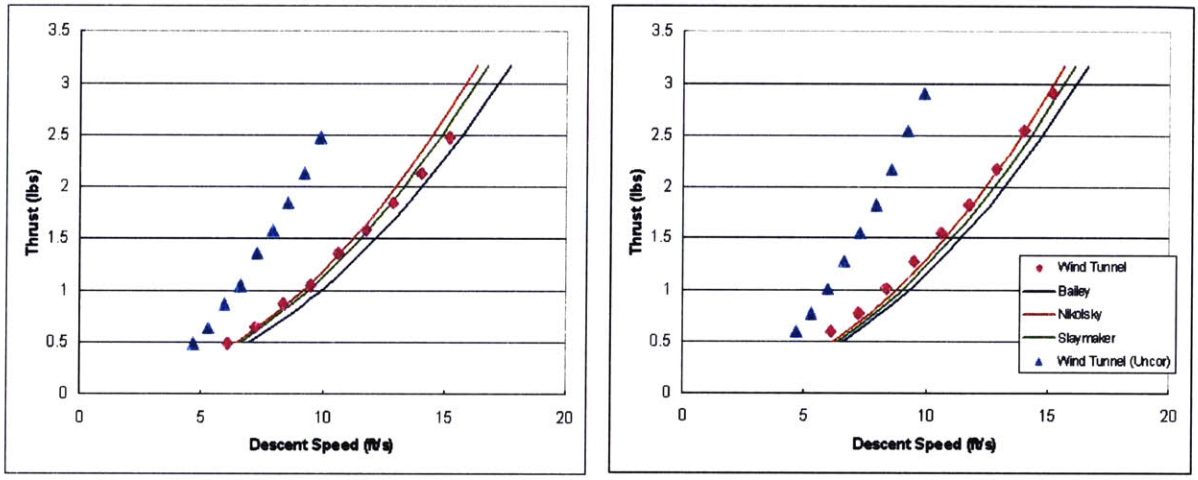

(a) Two bladed rotor

(b) Three bladed rotor

Figure 5-5: Thrust produced versus descent speed.

The blue triangles display the original tunnel data before any corrections are applied. The magenta diamonds show the data after the blockage and friction corrections have been applied. These corrected points match up well with all three theoretical algorithms. The data corrections are applied as described in Section 3.1.4. Both the theoretical and experimental results show the expected parabolic increase of thrust with descent velocity. This indicates that a fixed rotor configuration produces a near constant drag coefficient, no matter what the descent velocity.

5.1.3 Equilibrium RPM

Aside from collecting thrust data, the vertical wind tunnel is also equipped to take RPM readings. As mentioned earlier it is important to have an accurate model of rotor RPM, as it affects both the structural design and overall performance of the system.

While all three theoretical algorithms predicted similar values for thrust and drag coefficient, the Slaymaker method predicted a much higher RPM than the Bailey and Nikolsky methods. Thus, the tunnel can be used to determine which method is most accurate. Fig. 5-6 shows both the theoretical predictions and experimental data collected for rotor RPM versus descent speed.

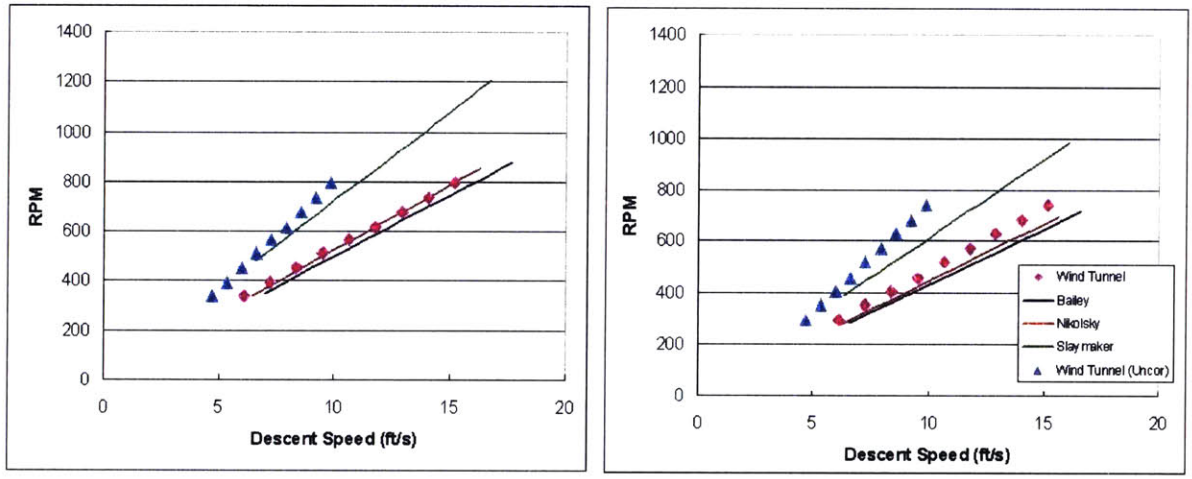

(a) Two bladed rotor **(b) Three bladed rotor**

Figure 5-6: RPM versus descent speed.

Whereas the thrust increases parabolically with descent speed, RPM increases linearly. This fact is validated by both the theoretical and experimental data. As far as accuracy is concerned, the corrected experimental data points, magenta diamonds, lie closer to the Bailey and Nikolsky theory, than the Slaymaker. This suggests that when predicting rotor performance, either the Bailey or Nikolsky theory should be favored.

Fig. 5-6 shows that the velocity correction works well on the RPM data. The uncorrected data, blue diamonds, show a much greater slope than the theoretical predictions. Also, a linear fit of the uncorrected data would not approach the origin where RPM should equal zero, but instead would cross $RPM = 0$ at $tunnelvelocity \approx 1.2$.

5.2 Parametric Analysis

Having determined that the wind tunnel results correlate well with the Bailey and Nikolsky predictions for a set rotor configuration, the correlation between experimental results and theory can be analyzed.

5.2.1 Drag Coefficient

Theoretically, it was predicted that the rotor drag coefficient would increase with increasing pitch up until the working state of the rotor was reached. At this point, c_{d_R} would level out around 1.2 and remain there until blade stall occurred, after which autorotation could no longer be achieved. The experimental data shows results in line with these predictions. Fig. 5-7 shows the the drag coefficient plotted against blade pitch for both the two and three bladed rotors. Included are the theoretical predictions found using the Bailey algorithm.

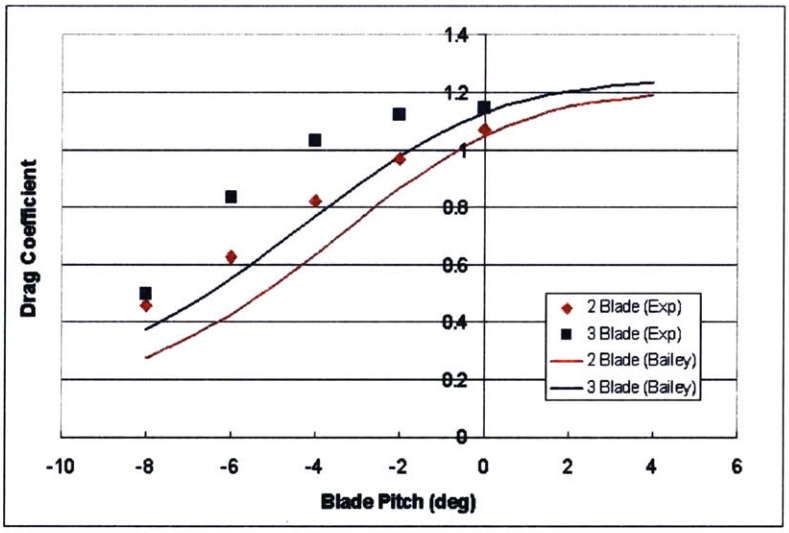

Figure 5-7: Drag coefficient versus blade pitch. Tunnel speed = 12 ft/s

The data points tend to match well. For instance, near the working state of the rotor, at 0^o blade pitch, there is almost no variation between the theoretical and experimental data. Even at its worst correlation, $\theta = -4^o$, the difference is less than

20%.

The experimental trend for both rotor configuration begins to become non-linear at -2^o blade pitch. This indicates that the rotor's have almost reached the working state, where c_{d_R} no longer increases.

Unfortunately, the experiments could never achieve full autorotation at blade pitches at the upper range of the working state. This is most likely due to two facts. One, although it is predicted that most rotors have a working state spanning from six to ten degrees [11], at low Reynolds numbers the increased drag may not allow for autorotation to occur very far into this range. At these Reynolds numbers, deviations in skin friction and flow quality can drastically increase the drag beyond what is predicted for smooth flow. Two, the start-up device used for this testing could only spin the rotor up to 500 RPM. It is possible that at $\theta > 0^o$ a much higher initial RPM is required to create stable autorotation. With these two points in mind, it can be said that a higher energy start-up device or higher Reynolds number tests may be able to show autorotation performance at higher blade pitches.

Comparing with the theoretical and experimental results shows that the collected data displays the same trends as theory. In both the theoretical and experimental data, the two bladed rotor produces a lower drag coefficient at the lower pitch settings. However, as pitch is increased the two and three bladed rotors begin to display similar drag coefficients.

5.2.2 RPM

Earlier, in Section 4.1.2, it was shown that the maximum RPM occurred well below the working state of the rotor, in the -20^o to -30^o range. However, those results were based on a free falling system where velocity and RPM increased until an equilibrium point was reached. In the wind tunnel, the velocity is held constant, allowing only the RPM to increase. This situation is similar to the portion of deployment when the autogyro is still attached to the parachute and causes the maximum RPM to occur at much higher pitch settings. Fig. 5-8 displays the rotor RPM for both the two and three bladed rotors, as a function of pitch.

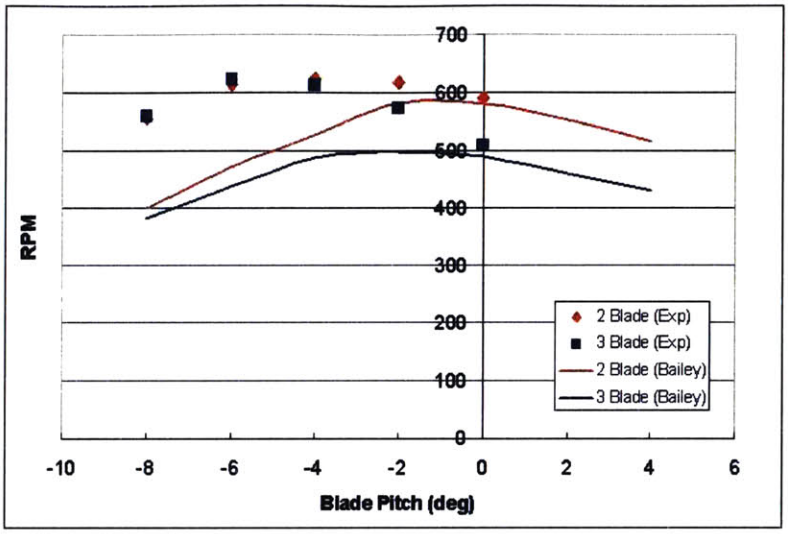

Figure 5-8: Rotor RPM versus blade pitch. Tunnel speed = 12 ft/s

In Fig. 5-8, the experimental data shows that RPM is similar for the both rotor types up until the maximum RPM is reached. At this point, the two bladed rotor begins to show a higher RPM value for a given pitch setting. The theoretical data shows similar trends. However, theoretically the maximum RPM for the two bladed rotor is 20% higher than for the three bladed rotor. This contrasts with the experimental data, which shows that both rotors achieve a similar maximum RPM.

5.2.3 Thrust Coefficient

The accuracy of the wind tunnel's calibration can be further analyzed by examining another non-dimensional parameter: the thrust coefficient, C_t. Unlike the drag coefficient, which is normalized by flow velocity, the thrust coefficient is normalized by RPM. Eliminating the velocity term is an enormous advantage since its accuracy is in doubt. The effects of blade pitch and rotor solidity on the thrust coefficient can be seen in Fig. 5-9.

Fig. 5-9 shows that the thrust coefficients for the three bladed rotor are actually lower than theoretically predicted. This indicates that for the given RPM, the rotor is not producing as much thrust as expected.

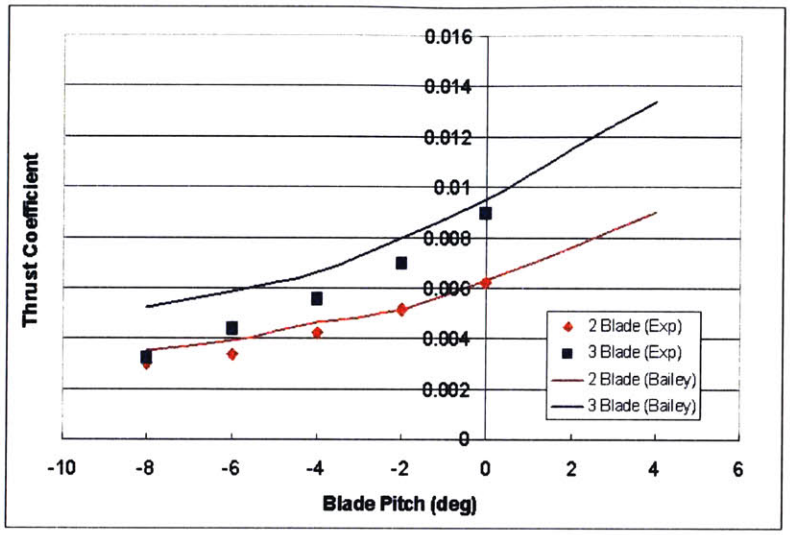

Figure 5-9: Thrust coefficient versus blade pitch.

5.3 Review of Tunnel Calibration

The previous sections have shown that the experimental and theoretical data match fairly well with each other. However, there are a few areas of concern which need to be addressed in order to better calibrate the tunnel.

Fig. 5-7 shows that at pitches from -8^o to -2^o, the experimentally collected drag coefficients for both the two and three bladed rotors were too high. Assuming the JR3 load cell is accurately calibrated, this fact implies that either the test section velocity is actually higher than expected or theory predicts drag coefficients which are low.

Theory shows that the RPM for the two bladed rotor should be higher than that of the three bladed rotor. However when looking at the RPM data in Fig. 5-8, the experimental data for the two rotors show similar results. Also, in the case of both rotors the overall RPM is higher than that predicted by theory.

From these various comparisons the following statements can be made:

- The experimentally collected drag coefficient is larger than predicted by theory.
- The experimentally collected rotor RPM is greater than predicted by theory.

- The RPM for the three bladed rotor is larger than predicted when compared against the two bladed rotor.

The first two statements point towards the fact that even after calibration, the equivalent velocity seen by the rotor is larger than predicted. If the tunnel velocity calibration coefficient were increased, it would have the effect of decreasing both the experimentally collected drag coefficient and rotor RPM. Also it appears that when the three bladed rotor is in the test section, it is seeing a higher equivalent velocity that the two bladed rotor would at the same tunnel setting. This fact can be seen in Fig. 5-8 where the three bladed rotor almost matches the RPM of the two bladed rotor.

These two errors seem to show that the blockage correction factor determined by the flat disk is slightly inaccurate. Both rotors increase the test section velocity more than the disk, and the three bladed rotor does so more than the two bladed rotor. It seems as if some phenomenon is occurring which is more complex than originally thought. Somehow the rotors are increasing the required correction by some means other than pure physical blockage.

One possible explanation is the differing nature of the aerodynamics of a disk and a rotor. Absolutely no flow pases through the disk. Thus, the velocity normal to the disk is zero at all points, and the flow must move tangent to the blockage to escape the tunnel.

On the other hand, when a rotor is placed in the tunnel, the blockage is not as uniform. On the inner portion of the rotor where the blades are moving slowly, there is little induced velocity. This allows some airflow to escape through the hub of the rotor. In contrast to this, the outer portions of the rotor blades are moving at a higher speed, and the induced velocity produced in this region is so large it actually causes a downwash effect. A basic diagram of the two flow patterns can be seen in Fig. 5-10.

The rotor blockage pattern is obviously more complicated than that caused by the flat disk, and due to its complexity it is hard to say if the rotor dynamics can be used to fully explain the error in the tunnel calibration. However, if future work is

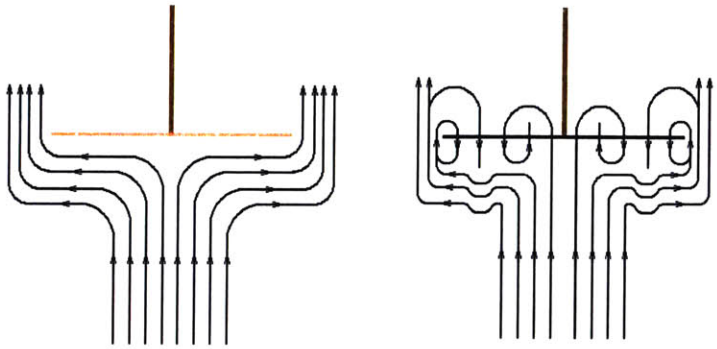

(a) Flow around disk (b) Flow around rotor

Figure 5-10: Flow around a flat disk(a) and rotor(b).

to be done to calibrate the tunnel, this may be one area on which the focus should initially be placed.

5.4 Dynamic Start-up

The initial concept for the wind tunnel did not include all of the instrumentation which made the performance analysis possible. Originally, the tunnel was designed to simply produce a vertical airflow, allowing for a qualitative analysis of start-up. As described in Ch. 2, the success of start-up is dependent upon two rotor parameters: blade pitch angle and initial RPM.

In an actual deployment scenario, the initial RPM is not only dependent on the rotor, but on the energy input device and its interaction with the body of the system. The amount of energy stored in the start-up device limits the initial system RPM, while the body design dictates how efficiently the stored energy is transferred to the rotor.

When the spring is released, and a torque is applied to the rotor mounted on the sting balance in the wind tunnel, the rotor torques back on the tunnel. Fortunately,

the tunnel weighs over 500 lbs. and is mounted to the floor, so this torque is obviously incapable of spinning the tunnel. However during airdrop, the rotor will only be mounted to the body of the system, and both will hang freely from the deployment parachute. When a torque is applied to the rotor, an equal and opposite torque will be applied to the body of the system. As it is not nearly as large as the tunnel, the body will then begin to rotate in a direction opposite the direction of the rotor.

The speed of the body's rotation, and in turn the energy lost due to this rotation will depend on a few characteristics of the body. The most influential is the body's moment of inertia, I_B. The larger I_B is, the less the body will rotate while the torque is being applied, this will allow the energy input device to exert more of its energy spinning up the rotor. Another factor is the size of the vertical tail placed on the body. A larger vertical tail will provide more drag to counteract the rotation of the body, thus slowing its rotation and adding more energy to the rotor.

A side benefit of slowing the rotation of the body is that the control system will not have to spend time getting the large initial yaw rate under control. In airdrop, time is altitude, and time spent stabilizing the initial yaw rate results in a decrease in the range of the system.

The qualitative deployment scenarios were performed with a mock payload and tail configuration hung freely from a teflon cord. This simulated how the system would be attached to the deployment parachute. For documentation purposes, the various spin-up configurations were recorded on a digital video camera.

The digital appendix contains three videos of possible dynamic start-up scenarios. "working.wmv" is a start-up performed with the blade pitch set at -2^o. This setting provides decent rotor performance, as well as a reliable start-up procedure. "high-pitch.wmv" shows the start-up of a rotor set to a pitch of 8^o. Here the rotor has no chance of achieving autorotation in the desired direction and actually starts to spin backwards due to the decelerating conditions.

"lowpitch.wmv" shows the blade pitch set at -8^o. For this start-up no energy input source was required to induce autorotation, as the aerodynamic forces alone provided enough torque to spin-up the rotor. Thus, the body was not given an initial

yaw rate. This is a major benefit of having a rotor with collective. The blades can be pitched down to start-up the rotor without spinning the body, then later pitched up to provide better performance.

The three videos demonstrate the concepts defined in Fig. 2-4 on page 30. "working.wmv" can be related to the yellow line, "highpitch.wmv" to the red line, and "lowpitch.wmv" to the green line. Overall the dynamic spin-up scenarios performed in the wind tunnel proved that autorotation can be achieved with a fixed pitch rotor in the working state, but if collective is available the deployment process is simplified.

[This page intentionally left blank.]

Chapter 6

Conclusions

6.1 Conclusions

The goal of this project was to answer three questions:

- What type of flight performance can be achieved by a gliding autogyro?
- What is the added benefit of including collective control in the rotor hub design?
- Can a fixed pitch rotor can be deployed with its blade pitch set in the rotor "working state"?

During the course of this project, the first question was examined in terms of rotor solidity, i.e. blade count, and blade pitch.

The issue of blade count has a direct answer. Three blades should be used. In all performance scenarios, the three bladed rotor outperformed the two bladed rotor. In vertical flight, the three bladed rotor had slower descent speeds and lower RPM values as can be seen in Sections 4.1.2, 4.1.2, 5.1.3, and 5.1.2. In forward flight, the three bladed rotor had a better minimum descent speeds and equivalent maximum lift-to-drag ratio as was shown in Sections 4.2.3 and 4.2.2. Finally, Section 4.3 showed that during flare, the extra inertia contained in the three bladed rotor provided for significantly better performance than that shown by the two bladed rotor.

Blade pitch is a much more complicated subject. In vertical descent, a blade pitch set in the working state of the rotor is desired to decrease the descent speed.

However, in forward flight, setting the blade pitch in the working state decreases the lift-to-drag ratio and overall flight speed. Also, deployment of the rotor is simplified by decreasing the blade pitch. This discussion leads directly into the second research question.

In every flight regime it was shown that adequate performance could be obtained using a fixed pitch rotor, but the performance could be improved if collective was added. With collective, the pitch could be adjusted to provide optimum performance during each stage of flight. Basically, the entire start-up process could be simplified. Not only would the need for a pre-rotation device be eliminated, but the initial yaw rate caused by that device would be removed as well. As a final thought, without collective the vertical landing flare would be impossible.

The decision to design and implement a rotor equipped with collective truly comes down to two questions: how much extra cost is involved and is the extra performance necessary? Before any final decision is to be made, an accurate assessment of the cost of designing and implementing a hub outfitted with collective should be performed. If the cost is reasonable, the added benefits of pitch control would improve system performance.

The third research question addresses the overall feasibility of the project. If the rotor cannot be made to achieve autorotation, there is no reason to analyze the system's performance. Fortunately, it was shown both theoretically and experimentally that rotor can achieve autorotation with a reasonable amount of energy input.

Theoretically, it was predicted that stable autorotation could be achieved at blade pitch values up to 8^o. However, due to limitations in the energy input source, the simulated parachute deployment process could only achieve reliable start-ups at $\theta = -2^o$. At that pitch there is a slight drop off in flight performance, but not significant enough to affect the feasibility of the project.

6.2 Future Work

If more time and funds were available, there are three main areas that needed to be further addressed. The first is determining how much it would cost to add collective to the rotor. Currently, there are a number of model helicopter rotor hubs equipped with collective for two blades. Using that as a starting point, it would have been useful to design a three bladed hub with collective. Obviously, designing, manufacturing, and instrumenting the prototype hub would have been costly, but having the ability to perform experiments such as simulated flares and stall boundary determinations would have shed light on the performance in certain flight regimes.

The second issue that could be addressed is the wind tunnel calibration. Although a large amount of time and effort were spent improving the flow quality, the final tunnel velocity settings still are in question. Obviously the tunnel blockage is a significant obstacle to overcome in determining the exact flow velocity the rotor is seeing, but more accurate values would allow for more in depth experiments.

Finally, other parameters need to be addressed in reference to system performance. Although blade pitch and blade count were studied thoroughly in this report, important parameters such as chord length and airfoil cross section were for all practical purposes ignored. Using the algorithms included on the digital appendix, the theoretical effects of these parameters could be discovered. The actual blades necessary to perform these experiments in the wind tunnel do not currently exist and would have to be either bought or constructed from scratch.

[This page intentionally left blank.]

Appendix A

Generic System Parameters

Parameter	Value
System Weight	3 lbs.
Rotor Radius	21.25 in
Blade chord	1.73 in
Zero Lift AOA	-5.1^o
Lift Curve Slope	5.79 rad^{-1}
Drag Polar	0.0602 - .04764α + 1.6795α^2 (α in rad)

Table A.1: Generic system parameters

[This page intentionally left blank.]

Appendix B

Contents of Digital Appendix

B.1 Data

Tests.xls

A Microsoft Excel spreadsheet which contains the raw data from all of the wind tunnel experiments. Included are thrust produced and RPM values for a number of different rotor configurations. All data was collected in the Draper Vertical Wind Tunnel.

B.2 Performance Prediction Algorithms

BaileyConstantPitch.m

A MATLAB m-file which calculates equilibrium descent conditions based on Bailey's tables. By fixing the pitch value for the rotor, the equilibrium descent velocity and RPM for vertical descent can be found for systems of varying weights. Requires the function 'bailey.m'. Based on NACA Report 716[4] and NACA Technical Note 1906.[18]

BaileyVaryPitch.m

A MATLAB m-file which calculates the equilibrium thrust and RPM based on a given wind tunnel velocity. This file also uses Bailey's tables and requires the function

'bailey.m' (see Section B.2.1). Based on NACA Report 716[4] and NACA Technical Note 1906.[18]

Flare.m

A MATLAB m-file which predicts the descent rate achieved over time for a collective flare maneuver. Based on NACA Technical Note 2870.[22]

ForwardFlight.m

A MATLAB m-file which predicts the forward flight performance of a given autogyro system based on input parameters. Utilizes theory from NACA Report 716.[4] Requires the functions: 'bailey.m', 'equil1.m', and 'equil2.m'.

NikolskyConstantPitch.m

A MATLAB m-file which calculates equilibrium descent conditions based on Nikolsky's algorithm for vertical descent. By fixing the pitch value for the rotor, the equilibrium descent velocity and RPM can be found for systems of varying weights. Based on NACA Technical Note 1906.[18]

NikolskyVaryPitch.m

A MATLAB m-file which calculates the equilibrium thrust and RPM based on a given wind tunnel velocity. It utilizes the Nikolsky algorithm and is Based on NACA Technical Note 1906.[18]

SlaymakerConstantPitch.m

A MATLAB m-file which calculates equilibrium descent conditions based on Slaymaker's algorithm for vertical descent. By fixing the pitch value for the rotor, the equilibrium descent velocity and RPM can be found for systems of varying weights. Based on NACA Technical Note 2870.[22]

SlaymakerVaryPitch.m

A MATLAB m-file which calculates the equilibrium thrust and RPM based on a given wind tunnel velocity. It utilizes the Slaymaker algorithm and is Based on NACA Technical Note 2870.[22]

B.2.1 Functions

bailey.m

A MATLAB function which can output the Bailey's coefficients based when provided the proper input parameters.[4]

equil1.m

A MATLAB function which is used to determine equilibrium in forward flight. Body drag is not included.

equil2.m

A MATLAB function which is used to determine equilibrium in forward flight. Body drag is included.

B.3 Sensors

rpmcollect.m

A MATLAB m-file which initializes, starts, and collects data from the RPM and load cell in the Draper Wind Tunnel. This file requires the MATLAB Data Acquisition Package. User must adjust the collection time prior to beginning a test, as well as zero out the JR3 load cell.

rpmanalyze.m

A MATLAB m-file which analyzes the data collected in 'rpmcollect.m'. Output is the a plot of RPM vs. time, as well as the loads and moments vs. time from the three axes of the load cell.

Tanalyze.m

A MATLAB m-file which further analyzes the data collected from the wind tunnel. By inputting time breaks and rotor angle of attack, this file will find the average thrust and horizontal force on the rotor over the given time period.

B.4 Videos

highpitch.wmv

A Windows Media Video file which shows the deployment sequence of a model autogyro whose blade pitch is set too high. Instead of achieving autorotation in the desired direction, the blades stall and the rotor begins to spin in the reverse direction.

lowpitch.wmv

A Windows Media Video file which shows the deployment sequence of a model autogyro whose blade pitch is set extremely low. It demonstrates how the rotor can achieve autorotation without the aid of a pre-rotator if the pitch is low enough. This system would give poor flight performance as the blade pitch is outside of the working state of the rotor.

working.wnv

A Windows Media Video file which shows the deployment sequence of a model autogyro whose blade pitch is set in the working state of the rotor. This video proves that a fixed pitch rotor can be spun-up in the working state where optimal flight performance occurs.

Bibliography

[1] Ira H. Abbott and Albert E. von Doenhoff. *Theory of Wing Sections.* Dover Publications, 1949.

[2] John D. Anderson. *Fundamentals of Aerodynamics.* McGraw-Hill, Inc., 1984.

[3] F.J. Bailey. A study of the torque equilibrium of an autogiro rotor. *NACA Report No. 623*, 1938.

[4] F.J. Bailey. A simplified theoretical method of determining the characteristics of a lifting rotor in forward flight. *NACA Report No. 716*, 1941.

[5] Glen Randall Bailey. *Guided parafoil system for delivering lightweight payloads.* U.S. Patent.

[6] Jewel B. Barlow, William H. Rae, and Alan Pope. *Low-speed Wind Tunnel Testing.* Wiley, 1999.

[7] Walter Castles and Robin B. Gray. Empirical relation between induced velocity, thrust, and rate of descent of a helicopter rotor as determined by wind tunnel testing. *NACA Technical Note 2474*, 1941.

[8] Juan de la Cierva and D. Rose. *Wings of Tomorrow: The Story of the Autogiro.* Brewer, Warren, and Putnam, 1931.

[9] Dictionary.com. *Online Dictionary.* www.dictionary.com, 2004.

[10] Extech. *Vane Anemometer*, 2004.

[11] Alfred Gessow and Garry C. Myers. *Aerodynamics of the Helicopters.* Frederick Unger Publishing Co., 1952.

[12] Sighard F. Hoerner. *Fluid Dynamic Drag: Practical Information on Fluid Dynamic Drag and Hydrodynamic Resistance.* Published by Author, 1958.

[13] JR3 Inc. *JR3 External Sensor Electronics with Digital Output*, 2003.

[14] Wayne Johnson. *Helicopter Theory.* Princeton University Press, 1980.

[15] Gordon C. Leishman. *In email.* 2004.

[16] J. Gordon Leishman. Development of the autogiro: A technical perspective. *Journal of Aircraft*, 2004.

[17] The Mathworks. *Data Acquisition Toolbox*, second edition, 1999.

[18] A.A. Nikolsky and Edward Seckel. An analytical study of the steady vertical descent in autorotation of single-rotor helicopters. *NACA Technical Note 1906*, 1949.

[19] Autogyro Company of Arizona. *Gyro Bee Conversion Kit*, 2003.

[20] American Society of Heating Refrigerating and Air conditioning Engineers. *ASHRAE Handbook: 1981 Fundamentals.* ASHRAE, 1981.

[21] Michael S. Selig. *Summary of Low-Speed Airfoil Data Vol. 3.* SoarTech Publications, 1997.

[22] S.E. Slaymaker and Robin B. Gray. Power-off flare-up tests of a model helicopter rotor in vertical autorotation. *NACA Technical Note 2870*, January 1953.

[23] J.B. Wheatley. An aerodynamic analysis of the autogiro rotor with a comparison between calculated and experimental results. *NACA Report No. 487*, 1935.